Aspects of Unusual Superconductivity

Thesis submitted for the degree of
Doctor of Philosophy (Science)

in

Physics (Theoretical)

by

Arghya Dutta

Department of Physics
University of Calcutta
July, 2014

This thesis is dedicated to

Holy Mother Sri Sarada Devi

Acknowledgments

First of all, I sincerely thank my thesis supervisor Prof. Jayanta K. Bhattacharjee. In academia, I am yet to meet another equally amazing person who epitomizes the definition of teacher, a friend, philosopher and guide, to such an extent. His deep physical insights, ability to do blazing fast calculations and superior intellect baffled, embarrassed and enlightened me, quite literally. I will not forget his benevolence, infinite patience and meticulous care while educating an inept student like me.

I am thankful to Prof. Manu Mathur for his generous helps in various administrative works during the absence of my supervisor. I am indebted to Prof. Amitabha Lahiri, Prof. Binayak Dutta-Roy and Prof Samir K. Paul for the excellent courses they offered during my M.Sc. years. I also sincerely thank Prof. S. S. Manna, Prof. Priya Mahadevan and Prof. Partha Mitra, of Saha Institute, for being in my thesis committee and providing encouragements during these five years. I thank Prof. Arup Kumar Raychaudhuri, director of our institute, for guiding me in third semester experimental project.

I am indeed lucky to have a collaborator like Dr. Sujoy Modak. We started collaborating while he was a Ph.D. student in this institute and it continues till date. It is a privilege to work with a good and industrious researcher like him. In this connection, I thank Prof. Thanu Padmanabhan of Inter-University Centre for Astronomy and Astrophysics (IUCAA) at Pune, India for granting me a visit to IUCAA in January, 2013.

Attending conferences and schools organized by International Centre for Theoretical Sciences (ICTS), Bangalore, India and Abdus Salam International Centre for Theoretical Physics (ICTP), Trieste, Italy has enriched me in myriad ways. I thank the organisers for generous funding and excellent arrangements.

My stay in the S. N. Bose national Centre for Basic Sciences has been a long one. I joined here as a post-B.Sc. student in August 2007. It is indeed amusing that I have spent seven years in this campus and I am happy and grateful for that. During this period, I met a number of wonderful friends. First I thank Soumyajit-da for numerous helps in LaTex as I must. He, incidentally, demanded an acknowledgement in the latex class file declarations he wrote! Debraj-da and Jena-da are two unique persons who never disappoint; I somehow suspect that the term "resourceful" was coined keeping them in mind and I am sorry for not returning, at least in equal measures, the favours I gladly received from them. I thank my group mates: Arnab-da, Raka-di, Amartya-da and Sukla for many helpful academic discussions. My seniors Debmalya-da, Abhijit-da, Prashant, Rudra-da, Hirak-da, Sudip-da, Tamoghna-da had been very generous to me, I thank them all. My juniors Subhashis, Arghya, Biplab, Arnab, Debanjan, Soumyadipta, Subhajit, Arindam, Arpan, Biswajit also kept the atmosphere sane and soothing, well, almost, if not always! My batch mates Ansuman and Atanu helped me a lot during the academically stressful M.Sc. years. I and Ansuman had been roommates for two years. During that time he started learning guitar and I pakhawaj.

We both developed a very agreeable habit of falling asleep while the other started his *riyaz*. That helped a lot in keeping our sanity intact.

During all these years in SNBNCBS, the non-academic staffs of this institute helped me in various ways. I specially thank the members of the library and academic section for being such nice persons. Also the cleaners and gardeners, probably the most hard-working persons of this centre, kept the campus beautiful, always.

I am indebted to the Council of Scientific and Industrial Research, India for financial support in the form of fellowship (File No.09/575(0062)/2009-EMR-1).

I am grateful to my parents, didibhai and Somnath-da for being so much supportive.

Finally, as it is, the deepest gratitude best remain unuttered, saying them belittles them and I prefer to refrain from doing it.

Arghya Dutta
Kolkata, India
July, 2014

List of Publications

The present thesis is based on the following publications:

In Journals:

1. **Arghya Dutta** and Jayanta K. Bhattacharjee
   Competing order parameters and a tricritical point with a difference
   Physica B, 407, 18, 3722-3726.

2. **Arghya Dutta** and Jayanta K. Bhattacharjee
   Lifshitz tricritical point and its relation to the FFLO superconducting state
   Physics Letters A, 377, 21-22, 1402-1406.

3. **Arghya Dutta** and Sujoy K. Modak
   Holographic entanglement entropy in imbalanced superconductors
   JHEP, 01, (2014), 136.

In Conference Proceedings:

1. **Arghya Dutta** and Jayanta K. Bhattacharjee
   Dynamical structure factor of Fulde-Ferrell-Larkin-Ovchinnikov superconductors
   AIP Conf. Proc. 1512, 1128 (2013).

Contents

List of Figures

Chapter 1

Introduction

1.1 Superconductivity

1.1.1 The phenomena

Superconductivity was discovered in 1911 by H. Kamerlingh Onnes [1] and physicists have the same zeal for understanding its manifold properties as they had a century before. On April 8th, 1911, H. K. Onnes, a staunch believer of the motto "knowledge through measurement" [2], with the help of his assistant Gilles Holst, observed that below a certain temperature T_c, later understood to be the critical temperature denoting a phase transition, the resistance of mercury, became *identically zero*. This finding was further bolstered by observing persistent currents in superconducting rings. Thus *perfect conductivity* is the foremost, and perhaps technologically most important, property of a superconductor. The next key property of a superconductor is *perfect diamagnetism* which causes the expulsion of magnetic field of lines out of a bulk superconducting material. But superconductivity has some more surprises to offer: when one cools a superconducting material from normal state to superconducting state, the magnetic field is automatically expelled from the bulk of the material.

This phenomenon is known as the Meissner effect. This effect is considered to be the defining character of a superconductor. The presence of such a reversible effect also demands that superconductivity will be destroyed if the applied magnetic field reaches a threshold value. This threshold value is known as critical magnetic field (H_c). The associated normal-superconductor phase transition is of second order at zero magnetic field, but becomes a first order transition in a finite magnetic field as the order parameter jumps and a latent heat is needed. In fact, depending on whether the magnetic field is completely expelled or allowed partially in the form of flux tubes, superconductors are divided in two major varieties: type-I and type-II. Meissner effect still remains an active field of research (See, for example, J. E. Hirsch [3]). After providing this brief introduction to superconductivity phenomena, in the next section we will discuss the path-breaking contribution of Bardeen, Cooper and Schrieffer in providing a microscopic theory of superconductivity.

1.1.2 Microscopic theory

The formulation of a microscopic theory of superconductivity remained an enigma for long and only after 40 years from its discovery, physicists started making progress in theoretical understanding of superconductivity. But the real breakthrough came with the theory proposed by Bardeen, Copper and Schreiffer. The fundamental mechanism responsible for superconductivity, according to their theory (now known as BCS theory), is the formation of Cooper pairs. In 1956 Cooper showed [4] that even an infinitesimal attractive interaction can form at least one bound pair of electrons in a Fermi sea. This result is counter-intuitive as in three dimensions, according to quantum mechanical laws, two bodies can form a pair only if the attraction between them reaches a minimum threshold value. But in this case Fermi statistics and the existence of a filled Fermi-sea make it possible for the electrons close to the Fermi

level to form Cooper pairs for arbitrarily weak interaction strength. Interestingly, attractive interaction between electrons results from the interactions of electrons with the quanta of lattice vibration, the phonons.

The seminal contribution of the justly famous BCS papers [5, 6] is that they explained the source of this attractive interaction between electrons in a metal and extended the two-body problem of Cooper pairs to a many-body problem and constructed the non-trivial ground-state wave function for the electrons. The variational ground-state many-body BCS wavefunction is:

$$|\psi\rangle = \prod_{\mathbf{k}} \left(u_{\mathbf{k}} + v_{\mathbf{k}} c^{\dagger}_{\mathbf{k}\uparrow} c^{\dagger}_{-\mathbf{k}\downarrow} \right) |0\rangle \tag{1.1}$$

where $|0\rangle$ is the vacuum state and $u_{\mathbf{k}}$ and $v_{\mathbf{k}}$ are variational parameters satisfying the constraint $u^2_{\mathbf{k}} + v^2_{\mathbf{k}} = 1$. The operator $c^{\dagger}_{\mathbf{k}\uparrow} c^{\dagger}_{-\mathbf{k}\downarrow}$ creates a Cooper pair with zero total momentum. The BCS theory predicted and explained some very important results like: 1) existence of an energy gap in the single-particle excitation unlike the normal metal, 2) the decrease of the gap with increasing temperature and becoming zero as T approaches T_c following the relation $\Delta \approx 1.74\Delta_0\sqrt{1-(T/T_c)}$, $\Delta_0 = 1.76 k_B T_c$ being the gap at $T = 0$, 3) the exponential fall-off of specific heat as $T \to 0$ etc. In the next section, we will describe a coarse-grained phenomenological model, formulated by Landau and Ginzburg [7] in 1950, which is an important alternative way to understand superconductivity and can be derived from the microscopic theory.

1.1.3 Phenomenological Ginzburg-Landau theory

As a theoretical model of superconductors, Landau and Ginzburg [7] formulated a phenomenological theory (hereafter GL theory) of superconductivity in 1950. They used Landau's innovative concept of writing down the free energy of a superconductor

as a power series expansion of the order parameter near the transition point of a second order phase transition. In physical terms, the complex order parameter is related to the density of Cooper pairs as $n(x) = |\psi(x)|^2$. The free energy, proposed by them, after considering symmetries of the problem, gauge invariance and variational principle, was:

$$F = F_n + a|\psi|^2 + \frac{b}{2}|\psi|^4 + \frac{1}{2m^*}\left|(-i\hbar\nabla - 2e\mathbf{A})\,\psi\right|^2 + \frac{|\mathbf{B}|^2}{2\mu_0}. \tag{1.2}$$

In this expression F_n is the free energy of the normal phase, a and b are phenomenological parameters. a is a function of temperature. m^* is some effective mass (it is the mass of the Cooper pairs, as it turned out later), $\mathbf{B}$ and $\mathbf{A}$ are magnetic field and corresponding vector potential, respectively. Though when first proposed GL theory was not appreciated that much, it got attention when Gor'kov showed [8] that the GL theory can be derived as a limiting form of BCS theory. The GL theory actually brings out the microscopic quantum-mechanical properties of the superconducting state. The GL theory also introduces a typical length scale, now known as GL coherence length which is defined by

$$\xi(T) = \frac{\hbar}{|2m^*\alpha(T)|^{1/2}}. \tag{1.3}$$

The coherence length characterizes the distance over which the superconducting order parameter can vary without any increase in energy. It is related to the Pippard coherence length at temperatures which are far below of the transition temperature. A superconductor has another length scale which Meissner effect supplies- the penetration depth(λ). The ratio of these two characteristics length scales defines the GL parameter $\kappa = \lambda/\xi$. Superconductors with $\kappa < 1/\sqrt{2}$ and $\kappa > 1/\sqrt{2}$ are known as type I and type II superconductors, respectively. In the first part of this thesis (chapters 2 and 3), we will explore imbalanced superconductors, explained in the next section, with the use of phenomenological GL free energy functionals and show

that they indeed explain experimental findings in ultracold atomic systems and two-dimensional organic superconductors.

1.2 Introduction of imbalance: Unusual states

In the previous two sections we have discussed superconductivity caused by zero center-of-mass momenta Cooper pairs (depicted in Fig. 1.1a) which are formed in presence of perfect balance in both number and the chemical potential of opposite spin electrons. As a natural extension of the BCS theory, physicists started wondering about superconductivity with imbalance either in population or in chemical potential of the spin-up and spin-down electrons. The existence of imbalanced superconductivity is an inherently interesting problem as spin polarization, and the resulting magnetism, destroys superconductivity. Clogston [9] and Chandrasekhar [10], in two independent works, first considered imbalanced superconductivity where imbalance in chemical potential of the spin-up and spin-down electrons comes from Zeeman coupling of the spin to an externally applied magnetic field and the orbital magnetism, and consequently the Meissner effect, is negligible compared to the Zeeman coupling. Clogston and Chandrasekhar found that above a certain value of chemical potential imbalance, or equivalently an applied external magnetic field (known as Clogston-Chandrasekhar or Pauli limit), the superconducting state becomes normal through a first-order phase transition. Now, there arises a difficulty in realizing this Pauli limit: In metals, superconductivity, or the absence of it, is controlled by orbital pair-breaking effects as the relevant upper critical field is much smaller than the Pauli limit and in that case, the physics is controlled by type-II superconductivity, not imbalanced superconductivity (For a detailed discussion on this competition between two limits, see the review by Matsuda et al [11]). So, Pauli limited superconductors are hard to

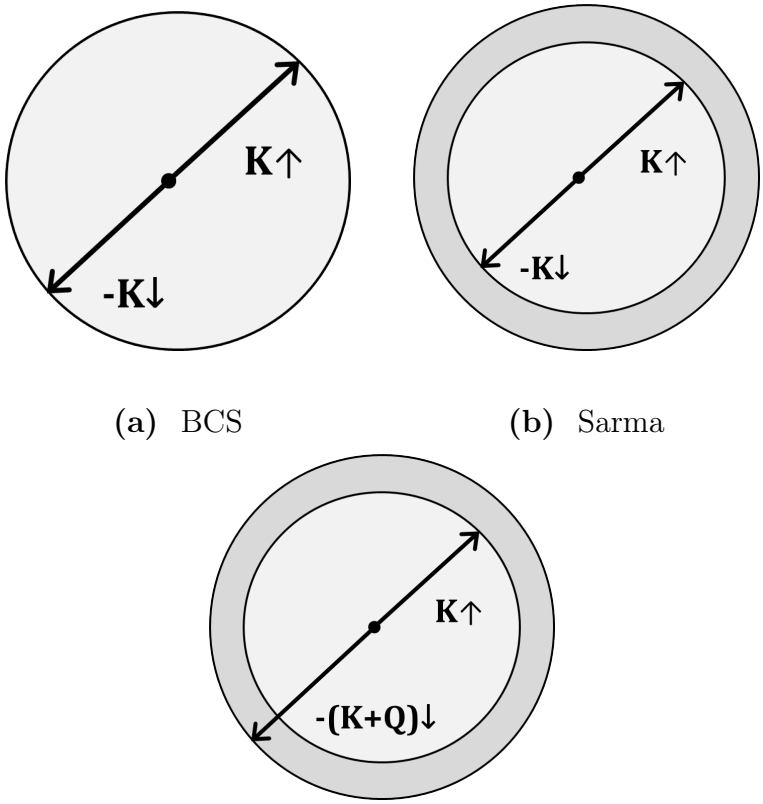

(a) BCS **(b)** Sarma

(c) FFLO

Figure 1.1 Formation of Cooper pairs in different scenarios. a) In the usual BCS picture, electrons at the Fermi surface form Cooper pairs with zero center-of-mass momenta. This changes when the density, equivalently chemical potential, of the spin-up and spin-down electrons becomes different. In this case: b) Sarma state may form with zero center-of-mass momenta Cooper pairs and thus opening a gap inside the Fermi sea of the majority electrons, or c) If Cooper pairs form with electrons from their respective Fermi surface, they acquire a momenta and FFLO state is formed. FFLO state has spatially-modulating order parameter, from the perspective of the phenomenological picture.

find and, therefore, should be tailor-made for verification of theoretical predictions. In the next two sections we will discuss two particular realizations of imbalanced superconductivity and contribution of the present thesis in better understanding these situations.

1.2.1 Sarma state

The theoretical details of a population imbalanced case and the corresponding first-order transition were first studied by Sarma in 1963 [12]. He showed that depending on the value of imbalance, an unstable superconducting state may appear in addition to the energetically stable normal state (see Fig. 1.1b). This intermediate phase is known as Sarma phase. The Sarma phase has attracted a lot of interest lately after the work by Liu et al [13]. The special characteristic of the Sarma phase is that it accommodates both superconducting and gapless phases at the same time. Though it has been shown to be an unstable phase [14] that conclusion, strictly speaking, holds only in the weak-coupling limit. When the scattering length becomes infinite, i.e. at unitarity, Quantum Monte Carlo simulations have demonstrated that the Sarma phase and the phase-separated BCS-normal state mixture are nearly degenerate in energy [15]. Also Sarma state is shown to be stable in presence of an optical lattice at moderate coupling [16]. In the chapter 2 of this thesis, we will explore the phase diagram obtained in a recent experiment by Shin et al [17] by means of phenomenological GL free energy and will show that an introduction of competing order parameters offers us a better understanding of the phase diagram than the picture offered by a standard tricritical theory which is traditionally used to describe a Sarma state.

1.2.2 FFLO superconductors

Just a year after Sarma's paper, in 1964 Fulde and Ferrell [18] and Larkin and Ovchhinikov [19] made a startling prediction about the possibility of a spatially inhomogeneous superconducting state at high magnetic field and low temperatures (See Fig. 1.1c). The new-proposed FFLO state was unique as it had a spatially-modulated order parameter, in contrast to the spatially-homogeneous order parameter of a standard BCS superconducting state. The FFLO state, other than being theoretically interesting, has major technological importance due to its high superconducting current densities and thus remains a very active field in both theoretical and experimental research till date.

From a theoretical perspective the FFLO state is quite intriguing as it retains its superconducting property overcoming the orbital and Pauli-paramagnetic pair-breaking effects, even at very high magnetic fields. Theoretical studies on the FFLO state are surprisingly wide-ranging as it has been vigorously studied for different physical systems like: crystalline colour superconductivity in dense quark matter [20], in Heavy-fermionic superconductors like $CeCoIn_5$ [11, 21], in ultracold imbalanced Fermi gas [22–24] and in optical lattice systems [25]. Though there is a dearth of systematic experimental studies, in ultracold atomic systems, in three dimensions, the generally reasonable agreement between theories and experiments suggests that the FFLO phase can occupy a small portion of the phase diagram. This is also true for certain solid state superconductors in the clean limit. In a related study [26], it was suggested that at low temperature the polaron gas could form p-wave superfluid, in accordance with Kohn-Luttinger theorem [27]. From 1980s, it is known [28, 29] that in lower dimensions, the chance of finding FFLO state is much higher as nesting of Fermi surface occurs. In the last decade, much effort has been given

to understand the formation of FFLO states in one dimension through bosonization methods [30,31], Bethe-ansatz calculations of the Yang-Gaudin model [32–34], Monte-Carlo approaches [35–37], DMRG analyses of the attractive Hubbard model or Yang-Gaudin model [38–44] and spin-DFT [45]. In the next section we will consider the present experimental situation.

1.2.3 Experimental findings

As discussed previously, Meissner effect makes difficult the experimental realization of a Sarma state or a FFLO state in superconductors. For this reason, the search for these states remains an area of active research by experimentalists. The experimental realization of imbalanced superconducting state can be achieved in two different kinds of systems: in ultracold Fermi gases and in solid state superconductors.

The use of ultracold gases as a test bed for realization of manybody quantum theories started after the methods of laser cooling and trapping of atoms were discovered. These methods led to the first observations of Bose-Einstein condensates of alkali vapours in 1995 [46, 47]. Following this development, the JILA group cooled down a fermionic atomic gas and observed quantum degenerate Fermi gases for the first time in 1999 [48]. In 2003 fermionic superfluidity was observed in ultracold systems [49–51]. Once balanced fermionic superfluidity was achieved, physicists started searching for imbalanced superfluids in spin-polarized Fermi systems and research groups from MIT [52] and Rice university [53] reported its observation in 2006. Though the results of the two groups were not in perfect agreement, they both agreed that there exists a superfluid state which is robust against spin imbalance. Many experiments soon followed after these pioneering experiments. Notably, of late, Liao et al [22] have studied trapped ultracold fermions in quasi-1D tubes and found some signatures of FFLO state.

The other way of experimental realization of the unusual superconducting states is the solid state superconductors. The prominent candidates among them are heavy-fermion superconductors like $CeCoIn_5$ and quasi two-dimensional organic superconductors. Recent advances in the heavy-fermion superconductors are made by Bianchi et al [54] and Radovan et al [55] who put forward thermodynamic evidences for the presence of FFLO state in $CeCoIn_5$. Besides this heavy-fermion superconductors, experiments done in the last decade on the quasi-two-dimensional organic superconductors have shown them to be promising candidates for exhibiting FFLO state [11, 56–58]. The advantage of these organic superconductors is that one can hugely suppress the orbital pair-breaking effect by applying magnetic field parallel to the highly conducting quasi-2D layers [58, 59]. The pioneering experiment was done by Singleton et al [60] for the organic superconducting material κ-(BEDT-TTF)$_2$Cu(NCS)$_2$ (BEDT-TTF is bisethylenedithio-tetrathiafulvalene) and the presence of the FFLO phase had been surmised from measurements sensitive to a loss in vortex stiffness. After that for λ-(BETS)$_2$GaCl$_4$ (BETS is bisethylenedithio-tetraselenafulvalene) a kink in the thermal conductivity [61] and in λ-(BETS)$_2$FeCl$_4$ a fall in the resistance [62–64] gave a hint about the existence of a FFLO state. But these results were somewhat inconclusive as they did not provide a rigorous thermodynamic evidence. The first clear thermodynamic evidence was observed by Lortz et al [65]. They found that a narrow intermediate superconducting state manifests itself at high magnetic field, applied parallel to the sample, of 21.5 Tesla and a first-order phase transition takes place. In chapter 3 we will see that a phenomenological GL free energy, derived from microscopic Hamiltonian, can explain the findings of this experiment and one can predict some new phenomena by doing a dynamical analysis of the proposed GL free energy.

1.2.4 Imbalance in holographic superconductor

The first two problems considered in this thesis essentially deal with imbalanced superconductors in the weak coupling limit. The theory of strongly coupled superconductivity, or for that matter any strongly coupled many-body quantum theory, is extremely difficult to formulate and understand. The study of strongly interacting many body systems started with the pioneering work of Bethe [66]. After that a wide class of solvable many-body systems was found in one dimensional systems. These systems are solvable, or integrable, in the sense that they have an infinite number of conservation laws and their wavefunctions can be written down using Bethe ansatz. However finding experimental realizations for these model systems and extending them to higher spatial dimensions turned out to be a hard work.

A novel approach for solving these strongly coupled systems is offered, surprisingly, by string theory. One of most notable concepts that emerged from the study of string theory is the gauge-gravity duality. This is an equivalence between a quantum field theory in d sapcetime dimensions and a quantum theory of gravity in $d+1$ spacetime dimensions. The gravity-free d-dimensional theory is a hologram of the $(d+1)$-dimensional theory in the sense that the number of degrees of freedom of the d-dimensional theory is equal to that of the $(d+1)$-dimensional theory with gravity. An important feature of this duality is that it also presents a strong-weak coupling duality: it maps a strongly-coupled theory in d dimensions (boundary) to a weakly-coupled theory in $(d+1)$ dimensions (bulk). Precisely for this reason it has generated a lot of interest in the condensed matter research community intent to comprehend new classes of strongly interacting field theory and a lot of work has been done already [67–70].

Of late, this newly found direction, hailed as AdS/CMT (anti-de Sitter - condensed

matter theory) correspondence, has got tremendous attention from both condensed matter and string communities. A new outcome of this field is the holographic superconductor which was first proposed by Hartnoll et al [71, 72]. The basic contention of them was that a minimal gravitational dual to a superconductor in $(2+1)$-dimensions can be obtained by coupling anti-de Sitter gravity to a Maxwell field and charged scalar field in $(3+1)$-dimensions. Using this formalism they showed that indeed a condensate forms below a certain critical temperature under some conditions. Calculation of frequency dependent conductivity also showed that a gap opens up for $T<T_c$ and addition of a magnetic field to the holographic superconductor demonstrated it to be a type-II superconductor. After this theoretical proposal of holographic superconductor, it was but natural to extend it to the imbalanced case and that was done by Erdmenger et al [73] and by Bigazzi et al [74]. In the spirit of studying unusual imbalanced superconductivity of this thesis, we have studied the behaviour of holographic entanglement entropy, an useful physical property, of this holographic imbalanced superconductor in chapter 4 and found some novel results.

1.3 Plan of the thesis

The present thesis is divided in three major chapters which are organized as follows:

In chapter 2, we propose a mean-field, phenomenological Ginzburg-Landau free energy functional with two competing order parameters to explain the experimentally observed properties [17] of a two-component, spin-polarized Fermi gas. This free energy supports a tricritical point which is different from the conventional one. The specific heat also happens to be different than in standard theory.

In chapter 3, we derive the phase diagram of FFLO superconducting state using the Ginzburg-Landau free energy. After describing its derivation from the microscopic

Hamiltonian of the system in detail, we notice that it has a very clear Lifshitz tricritical point. We find the specific heat jumps abruptly near the first-order line in the emergent phase diagram which is very similar to the recent experimental observation in layered organic superconductor [65]. We also show that the region of the phase diagram where the specific heat jumps can be probed by doing a dynamical analysis of the free energy.

In chapter 4, we study the behaviour of holographic entanglement entropy (HEE) of imbalanced holographic superconductors. To solve the problem, we employ numerical shooting method and consider the robust case of fully back-reacted gravity system. The hairy black hole solution, obtained using numerical method, is then used to compute the HEE for the superconducting case. The cases we study show that in presence of a mismatch between two chemical potentials, below the critical temperature, superconducting phase has a lower HEE in comparison to the AdS-Reissner-Nordström black hole phase. It is observed that the effect of chemical imbalance are different in the contexts of black hole and superconducting phases. For black hole, HEE increases with increasing imbalance parameter while it behaves oppositely for the superconducting phase. The implications of these results are discussed.

Finally, in the last chapter we will summarize our findings and state scope for future research.

Chapter 2

Competing order parameters and an unusual tricritical point

2.1 Introduction

As alluded to in the introduction, population imbalance between spin-up and spin-down fermions in a mixture of two Fermi gases leads to unusual superfluid phases. In past ten years, these exotic superfluid phases have been extensively studied, both theoretically by [13, 75–78] and experimentally [52, 53, 79–82] in different systems ranging from ultra-cold atomic gases to quark-gluon plasma which resides in the core of neutron stars [20, 56]. Similar imbalanced fermionic systems were studied in electron superconductors in a magnetic field as early as nineteen-sixties [12, 83], and showed the possibility of tricritical points where the second-order and the first-order lines meet along with the line separating stable and unstable superconducting phases. That the tricritical point is fundamental to the understanding of superfluidity of polarized, two-component Fermi gases was first pointed out by Parish et al [84]. In the next section we will provide a brief introduction to the tricritical point.

2.2 Tricritical point

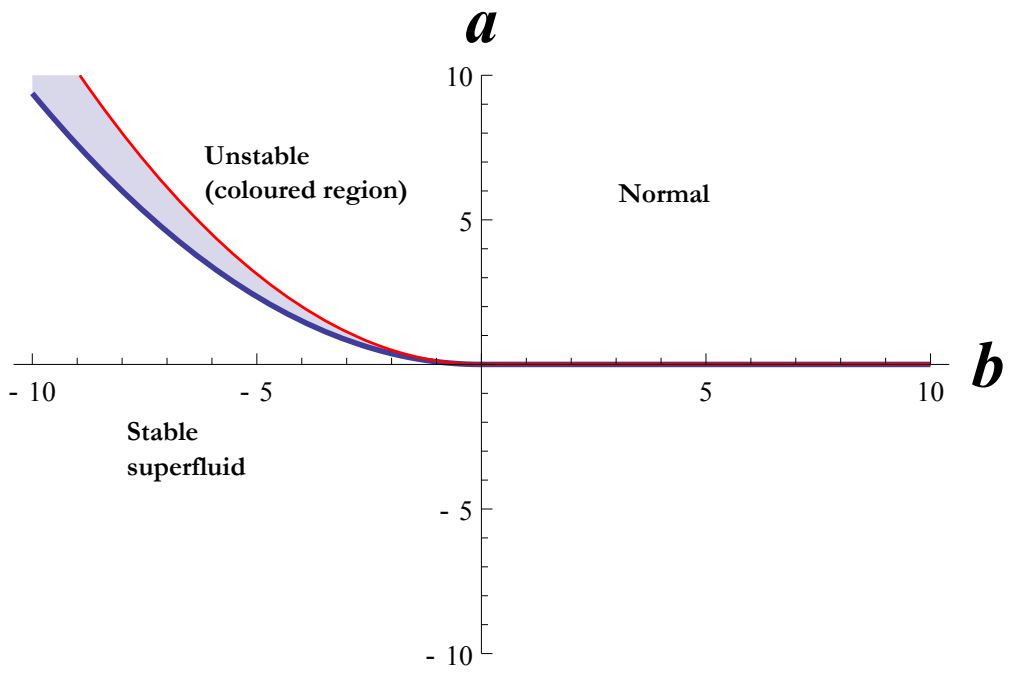

Figure 2.1 Standard $\mathcal{O}(\psi^6)$ theory phase diagram with scaled temperature (a) as x-axis and temperature-independent, polarization-dependent fourth order coupling constant(b) as y-axis. The shaded region represents a thermodynamically-unstable, finite-ψ region.

The standard model for studying tricritical point starts with the following Ginzburg-Landau free energy per unit volume

$$F = \frac{a}{2}\psi^2 + \frac{b}{4}\psi^4 + \frac{c}{6}\psi^6, \tag{2.1}$$

where ψ is superfluid order parameter, a is scaled temperature, c is a positive constant, and b can take both positive and negative values. Near the tricritical temperature(T_0), one usually expands a as a power series of temperature difference as $a = a_0(T - T_0)$ where a_0 is a constant and T is the temperature, and then searches for extrema in the free energy landscape. If all the coefficients of the free energy become positive then

F attains its minimum value at $\psi = 0$. In other words, the system remains in the normal state. For $b < 0$, however, the extrema of the free energy are located at those ψ-values which are solutions to the equation $a + b\psi^2 + c\psi^4 = 0$, specifically the non-zero minima are located at $\psi^2 = -b/2c \pm \sqrt{b^2 - 4ac}/2c$. Clearly a non-zero minimum exists if $b^2 > 4ac$. The minimum will be unstable energetically unless it satisfies $0 = F(\psi = 0) = F(\psi^2 = -b/2c + \sqrt{b^2 - 4ac}/2c)$, which happens if $ac = 3b^2/16$. So, in summary, in the free energy parameter space, we have an unstable finite-ψ phase between $a = 3b^2/16c$ and $a = b^2/4c$. The corresponding phase diagram is plotted in Fig. 2.1.

2.3 Recent experimental findings

Recently, an experiment by Shin et al [17] captured the first-order transition very clearly by measuring spatial discontinuity in spin polarization . In the experimental phase diagram reported by Shin et al [see Fig. 2.2], we note that the width of the unstable, finite-ψ region *increases with decreasing temperature*. It is, however, apparent that whatever polarization dependence we assign to the temperature-independent constant b of the standard $\mathcal{O}(\psi^6)$ theory, the width of the unstable superfluid region *decreases with decreasing temperature*.

2.4 Formulation of free energy

Keeping this discussion in mind, we set out to reconstruct[1] the free energy of this imbalanced Fermi system following the work done on antagonistic order parameter in superconductor-ferromagnet phase transitions, several decades ago by Blount et

[1]The work reported here is based on the paper "Competing order parameters and a tricritical point with a difference", Arghya Dutta and Jayanta K. Bhattacharjee, Physica B, **407**, 18, 3722-3726.

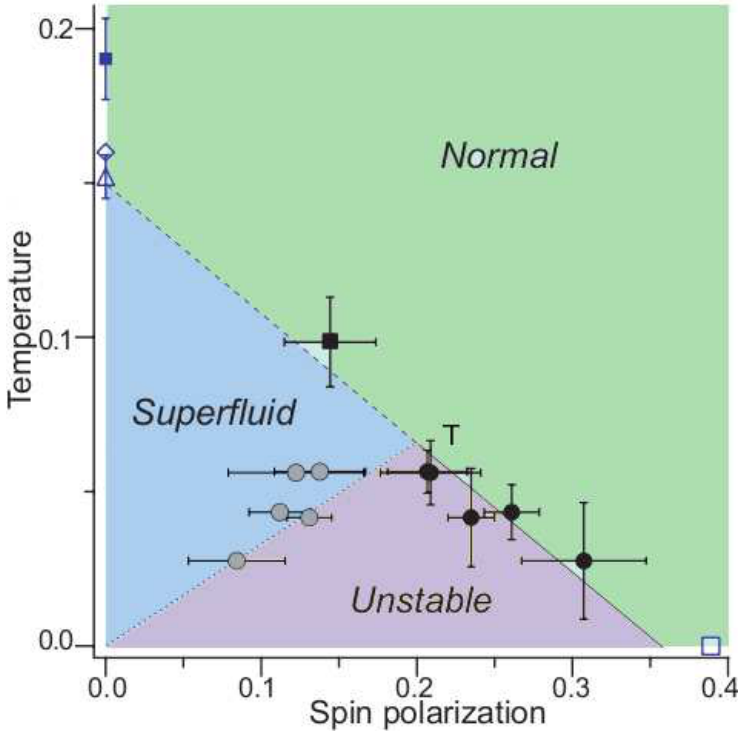

Figure 2.2 Relevant portion of the phase diagram of spin-imbalanced, two-component Fermi gas, as reported by Shin et al (Nature,2008) [17]. The point "T" denotes the tricritical point. The most important characteristics, which we are trying to point out in this work, is that the width of the unstable region (shaded violet) increases with decreasing temperature, whereas the width of the unstable region, as obtained from a standard $\mathcal{O}(\psi^6)$ theory, decreases with decreasing temperature, as can be seen in Fig. 2.1.

al [85]. Our phenomenological model free energy is a general Ginzburg-Landau type free energy with two order parameters, which are actually embedded in the system: one superconducting(ψ), and another imbalance parameter(m). This free energy explains the phase diagram properly and offers some valuable physical insights about imbalanced Fermi systems.

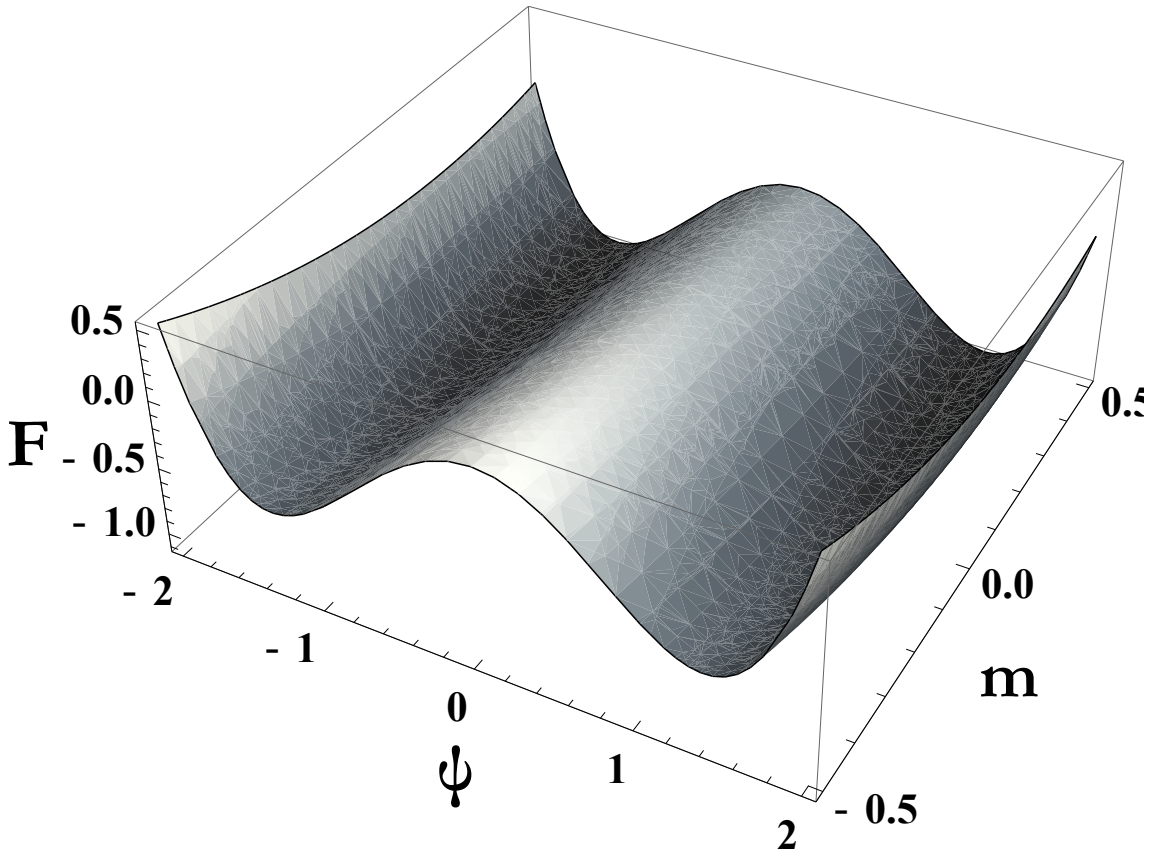

Figure 2.3 This figure depicts our model GL free energy(F) as a function of ψ and m. It clearly shows the double minima of F with respect to ψ and one minimum for m.

Our model free energy per unit volume is

$$F = \frac{a}{2}\psi^2 + \frac{b}{4}\psi^4 + \frac{A}{2}m^2 - mh + \frac{B}{2}m^2\psi^2 \tag{2.2}$$

in which ψ is superfluid order parameter, a is given by $a = a_0(T - T_C)$ where a_0

is a constant and T_C is the normal-superfluid transition temperature in absence of any imbalance. The parameter b is a temperature independent constant. As usual in mean field theory, we have a uniform superfluid state for $T < T_C$ with $\psi^2 = -a/b$. The imbalance parameter(m) is the difference in the number of spin-up and spin-down fermions. This parameter represents magnetization in the superconducting scenario and polarization in the ultra-cold atomic gas. Following the standard Ginzburg-Landau formalism, we include a term proportional to m^2 in the free energy (where the coefficient A is a constant) and the magnetic field (here chemical potential difference between the fermionic species) gives rise to an additional contribution $-mh$. We have neglected $\mathcal{O}(m^4)$ terms in the free energy as high imbalance destroys superfluidity. Finally, the $m^2\psi^2$ term, proposed after considering the symmetries of the system, signifies the interaction of the imbalance parameter with the superfluid order parameter. One has this freedom of choosing particular form of interaction while one is trying to explain the phase diagram of an imbalanced, two-species Fermi system at unitarity, because the particular functional form of the interaction does not matter in this resonantly-interacting regime. We have plotted the free energy in Fig. 2.3.

Here we need to say something about the underlying microscopic theory to make the results somewhat quantitative. To this end, we connect the proposed free energy to the available microscopic calculations of the system [83]. The microscopic calculation was done for a superconductor with an internal magnetic field generated by dilute magnetic impurity ions, neglecting the orbital effects, which is a justified assumption in a two-dimensional superconductor. The magnetic field differentiates between spin-up and spin-down electrons and thus creates an imbalance. From Maki's calculation (See Eq. (23) in Maki et al [83]), we get that the coefficient of the fourth order term(in ψ) the free energy expansion is given by $-[(mp_0)/(8\pi^2(2\pi T)^2)]Re\sum_{n=0}^{\infty}(n+\frac{1}{2}+i\rho)^{-3}$ where m, p_0 are the mass and Fermi momentum of the electron, respectively, and

$\rho = \mu H/2\pi T$. Near the tricritical point, we can approximate the above quantity to $-0.002mp_0$ after some algebra. In our theory, an expansion of the free energy in powers of ψ^2 gives the coefficient of the fourth order term to be $-(B^2/2A^3)(bA^3/2B^2 - h^2)$ which can be approximated as $-(bB^2/2A^3)^{\frac{1}{2}}$ near the tricritical point. So we can put the following condition on the phenomenological coefficients of our theory $\left(\frac{bB^2}{2A^3}\right)^{\frac{1}{2}} = 0.002mp_0$. We want to mention that as Maki's calculation was based on superconducting system, so this estimation is valid only in the deep-BCS limit. More recently, Sheehy [86] had done a similar calculation.

2.5 Phase diagram

To derive results for this model, we first minimise the Ginznurg-Landau free energy. Minimization results in two conditions on the order parameter

$$\bar{m} = h/(A + B\psi^2) \tag{2.3}$$

$$\psi(a + b\psi^2 + B\bar{m}^2) = 0. \tag{2.4}$$

Now for superfludity to be present in the system, one needs to solve the above equations simultaneously for non-zero solutions of the superfluid order parameter, and that is equivalent to solving

$$(a + b\psi^2)(A + B\psi^2)^2 + Bh^2 = 0. \tag{2.5}$$

This result can also be derived in a different way. We can integrate out the m-variable from Eq. (2.2), leading to an effective free energy F_{eff} which is different from the standard $\mathcal{O}(\psi^6)$ theory. The calculation goes like this:

$$\begin{aligned} e^{-F_{\text{eff}}} &= \int \mathcal{D}m e^{-F[m,\psi]} \\ &= \int \mathcal{D}m e^{-\left(\frac{a}{2}\psi^2+\frac{b}{4}\psi^4+\frac{A}{2}m^2-mh+\frac{B}{2}m^2\psi^2\right)} \\ &= \text{const} \times e^{-\left(\frac{a}{2}\psi^2+\frac{b}{4}\psi^4-\frac{h^2}{2(A+B\psi^2)}\right)}. \end{aligned} \tag{2.6}$$

So the effective free energy reads

$$F_{\text{eff}} = \frac{a}{2}\psi^2 + \frac{b}{4}\psi^4 - \frac{h^2}{2\left(A+B\psi^2\right)}. \tag{2.7}$$

As an interesting aside, we note that we can recover the standard $\mathcal{O}(\psi^6)$ free energy from this effective free energy by expanding F_{eff} near transition, where the value of ψ is small:

$$F_{\text{eff}} = -\frac{h^2}{2A} + \left(\frac{a}{2} + \frac{Bh^2}{2A^2}\right)\psi^2 + \left(\frac{b}{4} - \frac{B^2h^2}{2A^3}\right)\psi^4 + \frac{B^3h^2\psi^6}{2A^4} + O[\psi^8] \tag{2.8}$$

Now minimisation of the effective free energy with respect to ψ gives:

$$\begin{aligned} &\frac{\partial F_{eff}}{\partial \psi} = 0 \\ \Rightarrow\ &\psi\left[(a+b\psi^2)(A+B\psi^2)^2 + Bh^2\right] = 0, \end{aligned} \tag{2.9}$$

which is same as Eq. (2.5) for non-zero ψ. So, we have shown that the non-zero solutions of superfluid order parameter will be given by the solutions of Eq. (2.5). This shows that results from conventional tricritical point can differ when ψ^2 is not small and our contention is to show that this is the point of difference from standard tricritical point.

From Eq. (2.5), we note that the superfluid order parameter vanishes *continuously* along the curve $A^2a + Bh^2 = 0$. For temperatures greater than the tricritical temperature, a second order phase transition takes place as one crosses this curve to go from a normal($\psi = 0$) to a superfluid phase($\psi \neq 0$) or vice versa.

As our primary aim is to explain the phase diagram found by Shin et al, we will now check whether there exists a first order normal-superfluid transition in this system. If there exists a non-zero solution of the superfluid order parameter in the equation

$$F(\psi, \bar{m}) = F(\psi = 0, \bar{m}|_{\psi=0}), \tag{2.10}$$

there will be a first-order phase transition in the system. We insert our particular free energy in this equation and found the following values for the superfluid order parameter

$$\psi^2 = -\frac{1}{3}\left(\frac{A}{B} + \frac{2a}{b}\right) + \frac{1}{3}\sqrt{\left(\frac{A}{B} + \frac{2a}{b}\right)^2 - 6\left(\frac{aA}{bB} + \frac{h^2}{bA}\right)} \tag{2.11}$$

Using the functional form of ψ^2, we get two equations which relate the magnetic field and critical temperature : $h^2 = -aA^2/B$ and $h^2 = A(bA - 2aB)^2/8B^3$, across which a first-order normal-superfluid transition takes place. One of equations for the first order line is identical with the second-order line. The other curve is the purple line shown in Fig. 2.4. The tricritical temperature(T_0) can be easily determined by evaluating the intersection point of the two branches, which works out to be $a_0 = A\left[\left(\frac{b}{2B} - 1\right) \pm \sqrt{1 - \frac{b}{B}}\right]$. We designate this point as a tricritical point because it is the end point of a series of critical points, i.e., the order of the phase transition changes from second to first at this point.

Now let us figure out if there is any unstable region in the phase diagram within the scope of our model. This can be found out in this way- as we are treating this model at a mean field level, the phase of the superfluid order parameter is unimportant. Hence by demanding the square of the superfluid order parameter to be real, we find that there exist a unstable state for a range of temperature and magnetic field. According to the experimental data of Shin et al, in this region phase separation takes place. But from our free energy, which does not include any gradient term, we can

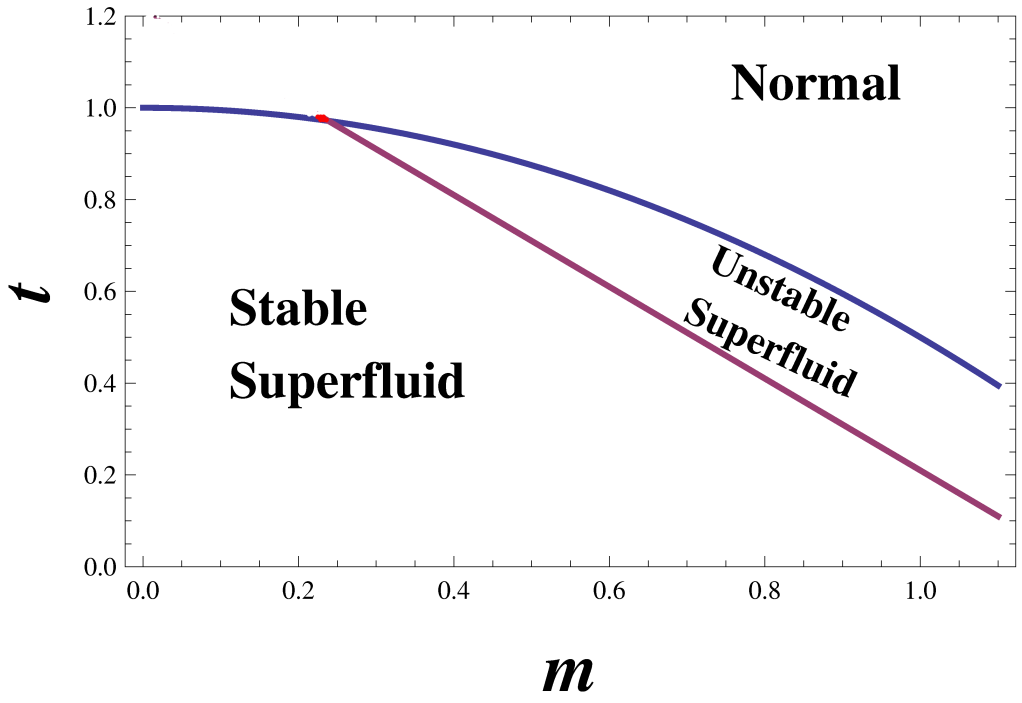

Figure 2.4 Spin polarization(m) vs. temperature($t = T/T_0$) phase diagram for an imbalanced two-component Fermi gas with resonant interactions. The area enclosed between the purple and blue line represents an energetically unstable region. The red dot is the tricritical point. For temperatures greater than the tricritical temperature superfluid-normal phase transition is second-order, while below it superfluid-normal phase transition is first-order which encounters an unstable phase en route. (Plotted using A=1.0, B=0.5 and b=0.2)

only conclude that this region is unstable.

2.6 Calculation of specific heat

Another interesting feature of this model Ginzburg-Landau free energy is its specific heat as we get a rather peculiar behaviour of this quantity near tricritical point.

Generally in $\mathcal{O}(\psi^6)$ theories, where tricritical point is quite generic, at temperatures just below tricritical point specific heat diverges as $C \sim a^{-\frac{1}{2}}$.

To calculate the specific heat of this our system, we differentiate twice the effective free energy (F_{eff}) with respect to a, which is nothing but scaled temperature, and we get

$$\begin{aligned} C &= \frac{\partial^2 F_{eff}}{\partial a^2} \\ &= \left(\frac{\partial \psi^2}{\partial a}\right) + \frac{a}{2}\left(\frac{\partial^2 \psi^2}{\partial a^2}\right) + \frac{b}{2}\left(\frac{\partial \psi^2}{\partial a}\right)^2 + \frac{b}{2}\psi^2\left(\frac{\partial^2 \psi^2}{\partial a^2}\right) \\ &- \frac{B^2h^2}{(A+B\psi^2)^3}\left(\frac{\partial \psi^2}{\partial a}\right)^2 + \frac{Bh^2}{2\,(A+B\psi^2)^2}\left(\frac{\partial^2 \psi^2}{\partial a^2}\right). \end{aligned} \tag{2.12}$$

So, as we can see from above equation, the nature of the specific heat is actually determined by the dependence of ψ^2 on a which can be extracted from Eq. (2.11). There are two distinct and interesting cases where the specific heat behaves differently.

Near transition point of the superfluid phase diagram, ψ^2 varies as a, in general, which can be derived from Eq. (2.11). If we put this a-dependence of ψ^2 in Eq. (2.12), we get $C = 1 + \frac{b}{2} + \frac{ba}{2} - \frac{B^2h^2}{(A+Ba)^3}$, which, near the transition point, becomes

$$C = 1 + \frac{b}{2} - \frac{B^2h^2}{A^3}. \tag{2.13}$$

So the specific heat have a jump discontinuity at the transition point. *We emphasise, this is different from the standard tricritical behaviour of specific heat, which actually diverges as we approach the tricritical point from lower temperatures.*

Now let us consider the second case. Interestingly, we can expand our free energy to get a $\mathcal{O}(\psi^6)$ theory. The coefficient of the ψ^4 term will be equal zero, which is required for a standard tricritical point, if $h_0^2 = \frac{bA^3}{2B^2}$ (from Eq. (2.8)). Now ψ will be proportional to $a^{1/4}$, like in standard tricritical theory, if we set $\frac{2|a|}{b} = \frac{A}{B} + \epsilon$, where ϵ is a small number and in that case ψ^2 reduces to

$$\psi^2 = \frac{\epsilon}{3} + \frac{1}{3}\sqrt{\epsilon^2 - 6\left(\frac{h^2}{bA} - \frac{A^2}{2B^2} - \frac{\epsilon A}{2B}\right)}. \tag{2.14}$$

Putting the value of h_0^2 in the above equation, we obtain $\psi^2 = \frac{\epsilon}{3} + \frac{1}{3}\sqrt{\epsilon^2 + \frac{3A}{B}\epsilon}$. As ϵ will tend to zero, ψ^2 will diverge as $\sqrt{\epsilon}$: finally we get the $\psi \sim a^{1/4}$ dependence. Doing a standard tricritical analysis we get $C \sim \left(a + \frac{Bh^2}{A^2}\right)^{-1/2}$, as expected. So indeed there is a point is the phase diagram, whose (a, h) coordinates are $\left(-\frac{Bh^2}{A^2}, \sqrt{\frac{bA^3}{2B^2}}\right)$, where we recover the standard tricritical behaviour.

Thus specific heat measurement will thus serve as an interesting check on whether the tricritical point is of the conventional type($\mathcal{O}(\psi^6)$ theory) or the findings over here. The main point of the last few paragraphs is that our model free energy encompasses the standard tricritical phenomena and, at the same time, points to some interesting physics which standard tricritical free energy does not account for. Now we want to make one final comment about the special case in which we set $b = B$ in our free energy. In this case, the transition point of our model and the standard tricritical point becomes one, and one can have $C \sim a^{-\frac{1}{2}}$, as in standard tricritical case, also for the transition point of our model.

2.7 Summary and discussion

To conclude, we have analysed the finite-temperature phase diagram of the two-component, imbalanced Fermi gas, as a function of population imbalance, using a phenomenological Ginzburg-Landau free energy. The novelty of our approach lies in using two order parameters, which, we assert, are actually embedded in the system: one superconducting and another imbalance order parameter. This approach is inspired by the Blount and Varma's Ginzburg-Landau free energy which was proposed to describe superconducting-ferromagnetic transition. Our analysis reproduces the phase diagram reported by experiment. We also point out that the specific heat behaves anomalously and provide a detailed analysis of the specific heat. We anticipate

that the proposed free energy, with two competing order parameters, will lead to improvements in our current understanding about the imbalanced Fermi gases.

Finally we mention one important point regarding the limitation this free energy. As our proposed free energy does not contain any gradient terms, it will not reproduce the Fulde-Ferrell-Larkin-Ovchinnikov(FFLO) [18, 19] superconducting state which is a superconducting state with a modulated order parameter. But one can extend this model free energy to include the gradient terms and study the FFLO state [87–89]. In the next chapter, we will do that analysis and will study the FFLO state in detail.

Chapter 3

Lifshitz tricritical point and FFLO superconductor: A study

3.1 Introduction

In 1964, Fulde and Ferrell [18] and Larkin and Ovchhinikov [19] envisaged a new kind of imbalanced superconductivity which is now known, after their name, as FFLO superconductor. As outlined in the introduction (see sections 1.2.2 and 1.2.3), the experimental realization of FFLO superconductor is difficult to achieve and the real implications of experiments claiming to observe the FFLO state remain a debated topic. To recapitulate, the experimental realization of FFLO state is difficult due to the stringent experimental conditions needed for it. The FFLO state only occurs if the superconductor is in the clean limit, i.e. the mean free path is much larger than the coherence length and the Maki parameter, a measure of the relative strength of orbital and Zeeman coupling to the external magnetic field, $\alpha = \sqrt{2}H_{orb}/H_P$ is greater than 1.8. The most promising candidates obeying these conditions are the heavy-fermionic superconductor $CeCoIn_5$ [54, 90–93] and layered, or quasi two-

dimensional(2D), organic superconductors.

The 2D organic superconductors have become the focus of late as they are, in most cases, clean superconductors and the orbital pair-breaking effect is mostly suppressed with a magnetic field applied parallel to the conducting layers. In an experiment done on the 2D organic superconductor κ-tetrathiafulvalene, Lortz et al [65] have provided a true thermodynamic evidence for an increase of the upper critical field and have shown the existence of a narrow intermediate superconducting region, which they have claimed to be a FFLO state. Recent magnetic torque [94] and nuclear magnetic resonance [95] measurements also support their view. Interestingly, one of the most prominent features marking the onset of the FFLO state is an anomalous jump in the specific heat [65,96]. This jump in specific heat marking the onset of FFLO state seems ubiquitous as it has been observed also in the heavy-fermionic superconductor $CeCoIn_5$ [54]. Though some very recent papers by Buzdin et al [97, 98] reported a study on anisotropic effects in 2D superconductors, the specific heat anomaly remains largely unexplored.

In this chapter[1] we present a theoretical study of the FFLO phase diagram with the help of GL free energy, derived from the microscopic Hamiltonian [56]. We calculate the specific heat to show that, indeed, the onset of the FFLO phase is accompanied by a jump in the specific heat across a first-order line. This jump is a direct consequence of the invariable presence of a Lifshitz tricritical point(LTP) in the FFLO phase diagram. The LTP occurs as a result of keeping the relevant [99] higher-order gradient terms in the GL free energy. The region in the phase diagram where the discontinuity in specific heat occurs can also be experimentally ascertained from a study

[1]The work reported here is based on the paper "Lifshitz tricritical point and its relation to the FFLO superconducting state", Arghya Dutta and Jayanta K. Bhattacharjee, Physics Letters A, **377**, 21-22, 1402-1406.

of the temporal behaviour of dynamical structure factor. We have shown this by suddenly quenching the system from the normal to the FFLO state across the LTP and calculating the structure factor using the time-dependent Ginzburg-Landau(TDGL) formalism. As a first step, in the next section, we will show the detailed derivation of the GL free energy for the sake of completeness.

3.2 Derivation of Ginzburg-Landau Free energy for FFLO superconductors

In this derivation of the free energy, which has been done previously by Buzdin et al [88] and Combescot et al [89], we will closely follow the notations and method used by Casalbuoni [56].

Let us start by considering an imbalanced fermionic gas formed by two fermionic species with different chemical potentials. They can be spin-up and spin-down fermions, or, in the case of imbalanced quark condensates, two quarks with different flavours. Let the chemical potential of the fermions are given by $\mu_u = \mu + \delta\mu, \mu_d = \mu - \delta\mu$. This imbalance in the two fermionic species can be described by adding a term to the system's Hamiltonian $H_{\text{imb}} = -\delta\mu\psi^\dagger\sigma_3\psi$, where σ_3 is the third Pauli matrix. The full action for this imbalanced system can be written as

$$\begin{aligned} S &= \int dt \frac{d\mathbf{p}}{(2\pi)^3}\, \psi^\dagger(\mathbf{p})\left(i\partial_t - E(\mathbf{p}) + \mu + \delta\mu\sigma_3\right)\psi(\mathbf{p}) \\ &\quad + \frac{g}{2}\int dt \prod_{k=1}^{4} \frac{d\mathbf{p}_k}{(2\pi)^3} \psi^\dagger(\mathbf{p}_1)\psi(\mathbf{p}_4)\psi^\dagger(\mathbf{p}_2)\psi(\mathbf{p}_3)(2\pi)^3\,\delta(\mathbf{p}_1 + \mathbf{p}_2 - \mathbf{p}_3 - \mathbf{p}_4) \end{aligned} \tag{3.1}$$

$\psi = (\psi_u, \psi_d)^T$ is a column matrix containing the annihilation operators of spin-up and spin-down fermions, respectively, and $E(\mathbf{p})$ is the dispersion relation of the fermions.

The action can be rewritten, in the mean-field approximation, as

$$\begin{aligned} S &= \int dt \, \frac{d\mathbf{p}}{(2\pi)^3} \, \psi^\dagger(\mathbf{p}) \left(i\partial_t - E(\mathbf{p}) + \mu + \delta\mu\sigma_3\right) \psi(\mathbf{p}) \\ &\quad -\frac{g}{4} \int dt \prod_{k=1}^{4} \frac{d\mathbf{p}_k}{(2\pi)^3} \left(\tilde{\Xi}(\mathbf{p}_3, \mathbf{p}_4) \psi^\dagger(\mathbf{p}_1) C \psi^\dagger(\mathbf{p}_2) - \tilde{\Xi}^*(\mathbf{p}_1, \mathbf{p}_2) \psi(\mathbf{p}_3) C \psi(\mathbf{p}_4) \right), \end{aligned} \tag{3.2}$$

where $C = i\sigma_2$ (σ_2 is the second Pauli matrix) and $\tilde{\Xi}(\mathbf{p}, \mathbf{p}') = \langle \psi(\mathbf{p}) C \psi(\mathbf{p}') \rangle$. In deriving the above, we have neglected the fluctuation terms like $(\psi^\dagger(\mathbf{p}_1) C \psi^\dagger(\mathbf{p}_2) + \tilde{\Xi}^*(\mathbf{p}_1, \mathbf{p}_2))$ and its complex conjugate, as one does in mean-field approximation while doing the standard BCS calculation. Now, to proceed, we introduce the Nambu-Gor'kov spinor

$$\chi(\mathbf{p}) = \frac{1}{\sqrt{2}} \begin{pmatrix} \psi(\mathbf{p}) \\ \psi^c(-\mathbf{p}) \end{pmatrix} \tag{3.3}$$

where ψ^c is the charge-conjugate field defined by $\psi^c = C\psi^\dagger$. We also introduce $\phi(\mathbf{p}, -\mathbf{p}')$ defined as

$$\phi(\mathbf{p}, -\mathbf{p}') = \frac{g}{2} \int \frac{d\mathbf{p}''}{(2\pi)^3} \tilde{\Xi}(\mathbf{p}'', \mathbf{p} + \mathbf{p}' - \mathbf{p}''). \tag{3.4}$$

In terms of the Nambu-Gor'kov spinor the action in Eq. (3.2) can be rewritten as

$$S = \int dt \, \frac{d\mathbf{p}}{(2\pi)^3} \frac{d\mathbf{p}'}{(2\pi)^3} \, \chi^\dagger(\mathbf{p}) \, S^{-1}_{NG}(\mathbf{p}, \, \mathbf{p}') \chi(\mathbf{p}'), \tag{3.5}$$

where

$$S^{-1}_{NG}(\mathbf{p}, \, \mathbf{p}') = (2\pi)^3 \begin{pmatrix} (i\partial_t - \xi_{\mathbf{p}} + \delta\mu\sigma_3)\delta(\mathbf{p} - \mathbf{p}') & -\phi(\mathbf{p}, \mathbf{p}') \\ -\phi^*(\mathbf{p}, \mathbf{p}') & (i\partial_t + \xi_{\mathbf{p}} + \delta\mu\sigma_3)\delta(\mathbf{p} - \mathbf{p}') \end{pmatrix}. \tag{3.6}$$

In this derivation we use $\xi_{\mathbf{p}} = E(\mathbf{p}) - \mu \approx \mathbf{v}_F.(\mathbf{p} - \mathbf{p}_F)$ in which $\mathbf{v}_F$ is the Fermi velocity. We can do this approximation because the Cooper Pair forming electrons come from the vicinity of the Fermi surface. The inverse Nambu-Gor'kov propagator

can be formally written as an operator as

$$S_{NG}^{-1} = \begin{pmatrix} (\mathbf{G_0^+})^{-1} & -\boldsymbol{\phi} \\ -\boldsymbol{\phi}^* & -(\mathbf{G_0^-})^{-1} \end{pmatrix}. \tag{3.7}$$

with $(G_0^+)^{-1} = E - \xi_p + \delta\mu\sigma_3 + i\epsilon\,\mathrm{sgn}E$ and $(G_0^-)^{-1} = -E - \xi_p - \delta\mu\sigma_3 - i\epsilon\,\mathrm{sgn}E$ with $\epsilon = 0^+$. The Nambu-Gor'kov propagator S turns out to be

$$S_{NG} = \begin{pmatrix} \mathbf{G} & -\tilde{\mathbf{F}} \\ -\mathbf{F} & \mathbf{G} \end{pmatrix}. \tag{3.8}$$

The solution for this system, obtained from Nambu-Gor'kov equation $S_{NG}^{-1}S_{NG} = \mathbb{1}$ is:

$$\mathbf{F} = \mathbf{G_0^-}\boldsymbol{\phi}^*\mathbf{G} \tag{3.9}$$

$$\mathbf{G} = \mathbf{G_0^+} - \mathbf{G_0^+}\boldsymbol{\phi}\mathbf{F} \tag{3.10}$$

so that $\mathbf{F}$ satisfies

$$\mathbf{F} = \mathbf{G_0^-}\boldsymbol{\phi}^*(\mathbf{G_0^+} - \mathbf{G_0^+}\boldsymbol{\phi}\mathbf{F}). \tag{3.11}$$

This is main equation necessary for deriving the free energy as a power series of the order parameter. The order parameter at finite temperature (T) can derived from the consistency condition

$$\phi^*(\mathbf{r}) = \frac{g}{2}T\sum_{n=-\infty}^{+\infty}\mathrm{Tr}F(\mathbf{r},\mathbf{r},E)|_{E=i\omega_n} \tag{3.12}$$

in which we have used the Matsubara frequencies $\omega_n = (2n+1)\pi T$. From now on we will consider a finite temperature superconductor, as it is indispensable to derive the finite temperature phase diagram and, subsequently, use finite temperature field theory techniques to derive results. The Ginzburg-Landau series for the propagator $\mathbf{F}$, from Eq. 3.11, reads

$$\mathbf{F} = +\mathbf{G_0^-}\boldsymbol{\phi}^*\mathbf{G_0^+} - \mathbf{G_0^-}\boldsymbol{\phi}^*\mathbf{G_0^+}\boldsymbol{\phi}\mathbf{G_0^-}\boldsymbol{\phi}^*\mathbf{G_0^+} + \mathbf{G_0^-}\boldsymbol{\phi}^*\mathbf{G_0^+}\boldsymbol{\phi}\mathbf{G_0^-}\boldsymbol{\phi}^*\mathbf{G_0^+}\boldsymbol{\phi}\mathbf{G_0^-}\boldsymbol{\phi}^*\mathbf{G_0^+}\ . \tag{3.13}$$

Let us now invoke the particular form of the gap given by $\phi(\mathbf{r}) = \sum_{m=1}^{P} \phi_m e^{2i\mathbf{k}_m.\mathbf{r}}$. The gap is proportional to the condensate wave function and its form is determined by the fact that there will be pairs with nonzero total momentum in a FFLO superconductor. The Ginzburg-Landau free energy can be determined from the interaction Hamiltonian and it is given by $\Omega = \int \frac{dg}{g^2} \int d\mathbf{x} |\phi(\mathbf{x})|^2$ (for a derivation, see Abrikosov et al [100], Chapter 7, Section 36). Using this and substituting the form of the FFLO order parameter from Eq. (3.13), the grand potential, in momentum space, turns out to be

$$\begin{aligned}
\Omega &= \frac{2}{g} \sum_{k,n} \left[1 - \Pi(\mathbf{k}_k, \mathbf{k}_n)\right] \phi_k^* \phi_n \delta_{\mathbf{k}_k - \mathbf{k}_n} \\
&- \frac{1}{g} \sum_{k,\ell,m,n} J(\mathbf{k}_k, \mathbf{k}_\ell, \mathbf{k}_m, \mathbf{k}_n) \phi_k^* \phi_\ell \phi_m^* \phi_n \delta_{\mathbf{k}_k - \mathbf{k}_\ell + \mathbf{k}_m - \mathbf{k}_n} \\
&+ \frac{2}{3g} \sum_{k,\ell,m,j,i,n} K(\mathbf{k}_k, \mathbf{k}_\ell, \mathbf{k}_m, \mathbf{k}_j, \mathbf{k}_i, \mathbf{k}_n) \phi_k^* \phi_\ell \phi_m^* \phi_j \phi_i^* \phi_n \delta_{\mathbf{k}_k - \mathbf{k}_\ell + \mathbf{k}_m - \mathbf{k}_j + \mathbf{k}_i - \mathbf{k}_n}.
\end{aligned} \tag{3.14}$$

In the above expression, Π, J, and K, which are products of Green's functions, are defined as:

$$\Pi(k) = -\frac{g\rho T}{2} \int \frac{d\hat{\mathbf{w}}}{4\pi} \int_{-\delta}^{+\delta} d\xi \sum_{n=-\infty}^{+\infty} \frac{1}{(i\omega_n - \delta\mu - \xi - 2\hat{\mathbf{w}} \cdot \mathbf{k} v_F)(i\omega_n - \delta\mu + \xi)}, \tag{3.15}$$

$$\begin{aligned}
J(\mathbf{k}_1, \mathbf{k}_2, \mathbf{k}_3, \mathbf{k}_4) = -\frac{g\rho T}{2} \int \frac{d\hat{\mathbf{w}}}{4\pi} \int_{-\delta}^{+\delta} d\xi \sum_{n=-\infty}^{+\infty} \prod_{i=1}^{2} \Big\{ &\frac{1}{i\omega_n + \xi - \delta\mu + 2\,\mathbf{w} \cdot \mathbf{q}_i} \\
&\frac{1}{i\omega_n - \xi - \delta\mu - 2\,\mathbf{w} \cdot \boldsymbol{\ell}_i} \Big\},
\end{aligned} \tag{3.16}$$

and

$$K(\mathbf{k}_1,\mathbf{k}_2,\mathbf{k}_3,\mathbf{k}_4,\mathbf{k}_5,\mathbf{k}_6) = -\frac{g\rho T}{2}\int\frac{d\hat{\mathbf{w}}}{4\pi}\int_{-\delta}^{+\delta}d\xi\sum_{n=-\infty}^{+\infty}\prod_{i=1}^{3}\Big\{\frac{1}{i\omega_n+\xi-\delta\mu+2\,\mathbf{w}\cdot\mathbf{q}_i} \\ \frac{1}{i\omega_n-\xi-\delta\mu-2\,\mathbf{w}\cdot\boldsymbol{\ell}_i}\Big\}. \tag{3.17}$$

In writing the above, we have defined

$$\begin{aligned}\mathbf{q}_1 &= \mathbf{0}, \quad \mathbf{q}_2=\mathbf{k}_1-\mathbf{k}_2, \qquad \mathbf{q}_3=\mathbf{k}_1-\mathbf{k}_2+\mathbf{k}_3\,,\\ \boldsymbol{\ell}_1 &= \mathbf{k}_1, \quad \boldsymbol{\ell}_2=\mathbf{k}_1-\mathbf{k}_2+\mathbf{k}_3, \quad \boldsymbol{\ell}_3=\mathbf{k}_1-\mathbf{k}_2+\mathbf{k}_3-\mathbf{k}_4+\mathbf{k}_5\,,\end{aligned} \tag{3.18}$$

with the conditions $\mathbf{k}_1-\mathbf{k}_2+\mathbf{k}_3-\mathbf{k}_4=0$ and $\mathbf{k}_1-\mathbf{k}_2+\mathbf{k}_3-\mathbf{k}_4+\mathbf{k}_5-\mathbf{k}_6=0$ for J and K respectively. ρ is the density of states at the Fermi level and δ is the energy cut-off.

3.2.1 Evaluation of $\Pi(k)$

Expanding the first denominator of $\Pi(k)$ in Eq. (3.15) in the momentum $\mathbf{k}$ we get

$$\Pi(k) = \frac{1}{2}g\rho T\sum_{n=-\infty}^{+\infty}\int\frac{d\hat{\mathbf{w}}}{4\pi}\int_{-\infty}^{+\infty}d\xi\sum_{m=0}^{\infty}\frac{1}{\bar{\omega}_n^2+\xi^2}\frac{(2\hat{\mathbf{w}}\cdot\mathbf{k}v_F)^{2m}}{(i\bar{\omega}_n-\xi)^{2m}}\,. \tag{3.19}$$

where $\bar{\omega}_n=\omega_n+i\delta\mu$.

Here the order of sum and integration is changed as first done by Buzdin et al [88] to make the final result more understandable from physical point of view. Now with the help of the integral

$$\int_{-\infty}^{+\infty}d\xi\frac{1}{\bar{\omega}_n^2+\xi^2}\frac{1}{(i\bar{\omega}_n-\xi)^{2m}} = (-1)^m\frac{\pi}{2^{2m}\bar{\omega}_n^{2m+1}}, \tag{3.20}$$

it is straightforward to derive that

$$\Pi(k) = \frac{1}{2}g\pi\rho T\sum_{n=-\infty}^{+\infty}\sum_{m=0}^{\infty}\frac{(-1)^m}{2m+1}\frac{k^{2m}}{\bar{\omega}_n^{2m+1}}. \tag{3.21}$$

In the above expression we have absorbed the fermi velocity in $\mathbf{k}$. Finally, we can now derive the coefficient of the term which is quadratic in order parameter in Eq. (3.14)

$$\begin{aligned}
&\frac{2}{g}(1-\Pi(k)) \\
&= \frac{2}{g} - \pi\rho T \sum_{n=-\infty}^{+\infty} \frac{1}{\bar{\omega}_n} + \frac{\pi\rho T}{3}k^2 \sum_{n=-\infty}^{+\infty} \frac{1}{\bar{\omega}_n^3} - \frac{\pi\rho T}{5}k^4 \sum_{n=-\infty}^{+\infty} \frac{1}{\bar{\omega}_n^5} \\
&= (\alpha + \frac{2}{3}\beta k^2 + \frac{8}{15}\gamma k^4). \qquad (3.22)
\end{aligned}$$

We have defined α, β and γ, which will appear frequently, as

$$\begin{aligned}
\alpha &= \frac{2}{g} - 2\pi\rho T \mathrm{Re} \sum_{n=0}^{+\infty} \frac{1}{\bar{\omega}_n} \\
&= \rho\left[\ln\left(\frac{4\pi T}{\phi_0}\right) + \mathrm{Re}\,\psi\left(\frac{1}{2} + i\frac{\delta\mu}{2\pi T}\right)\right] \qquad (3.23) \\
\beta &= \pi\rho T\,\mathrm{Re} \sum_{n=0}^{+\infty} \frac{1}{\bar{\omega}_n^3} \\
&= -\frac{\rho}{16\pi^2 T^2}\,\mathrm{Re}\left[\psi^{(2)}\left(\frac{1}{2} + i\frac{\delta\mu}{2\pi T}\right)\right] \qquad (3.24) \\
\gamma &= -\frac{3}{4}\pi\rho T\,\mathrm{Re} \sum_{n=0}^{+\infty} \frac{1}{\bar{\omega}_n^5} \\
&= \frac{3}{4}\frac{\rho}{768\pi^4 T^4}\,\mathrm{Re}\left[\psi^{(4)}\left(\frac{1}{2} + i\frac{\delta\mu}{2\pi T}\right)\right] \qquad (3.25)
\end{aligned}$$

where $\psi(z)$ and $\psi^n(z)$ are Euler function and its nth derivative, respectively. Here we should mention that the determination of first term (α) is a bit tricky, one needs to introduce an energy cut-off to regulate the divergent sum and then replace the cut-off by the gap parameter at zero temperature which is denoted here by ϕ_0 (see Buzdin et al [88]).

3.2.2 Evaluation of J and K

To evaluate J we need to introduce the Feynman variables x_j, y_j ($j = 1, 2$ for J and $j = 1, 2, 3$ for K) and form vectors $\mathbf{q} = \sum_i x_i \mathbf{q}_i$ and $\boldsymbol{\ell} = \sum_i y_i \boldsymbol{\ell}_i$. After introducing

them, J in Eq. (3.16) becomes

$$J(\mathbf{k}_1,\mathbf{k}_2,\mathbf{k}_3,\mathbf{k}_4) = -\frac{g\rho T}{2}\int\frac{d\hat{\mathbf{w}}}{4\pi}\int_{-\delta}^{+\delta}d\xi\sum_{n=-\infty}^{+\infty}\int\prod_{m=1}^{2}dx_m dy_m \frac{\delta(1-\sum x_m)\delta(1-\sum y_m)}{(i\omega_n+\xi-\delta\mu+2\,\mathbf{w}\cdot\mathbf{q})^2} \frac{1}{(i\omega_n-\xi-\delta\mu-2\,\mathbf{w}\cdot\boldsymbol{\ell})^2} \tag{3.26}$$

The energy integral is done by the method of residues and we expand the resultant integral in powers of momentum. The result is

$$J = -\frac{\pi\rho g T}{2}\left[\mathrm{Re}\sum_{n=0}^{+\infty}\frac{1}{\bar{\omega}_n^3} - 2\mathrm{Re}\sum_{n=0}^{+\infty}\frac{1}{\bar{\omega}_n^5}\int dx_m dy_m \delta(1-\sum x_m)\delta(1-\sum y_m)v_F^2|\mathbf{q}-\boldsymbol{\ell}|^2\right]$$

after some simplification which becomes

$$= -\frac{g}{2}\left(\beta+\frac{4\gamma}{9}\left(k_1^2+k_2^2+k_3^2+k_4^2+\mathbf{k}_1\cdot\mathbf{k}_3+\mathbf{k}_2\cdot\mathbf{k}_4\right)\right), \tag{3.27}$$

where we have used the definition of β and γ from Eq. (3.24) and Eq. (3.25) respectively and kept terms upto second order in momentum so that only gradient-square terms of the order parameter remain.

In exactly similar way K can be determined. The steps are as follows:

$$\begin{aligned} K &= -\frac{g\rho T}{2}\int\frac{d\hat{\mathbf{w}}}{4\pi}\int_{-\delta}^{+\delta}d\xi\sum_{n=-\infty}^{+\infty}\prod_{i=1}^{3}\Big\{\frac{1}{i\omega_n+\xi-\delta\mu+2\,\mathbf{w}\cdot\mathbf{q}_i} \\ &\quad \frac{1}{i\omega_n-\xi-\delta\mu-2\,\mathbf{w}\cdot\boldsymbol{\ell}_i}\Big\} \\ &= -g\rho T\int\frac{d\hat{\mathbf{w}}}{4\pi}\int_{-\delta}^{+\delta}d\xi\sum_{n=-\infty}^{+\infty}\int\prod_{m=1}^{3}dx_m dy_m \\ &\quad \frac{\delta(1-\sum x_m)\delta(1-\sum y_m)}{(i\omega_n+\xi-\delta\mu+2\,\mathbf{w}\cdot\mathbf{q})^3(i\omega_n-\xi-\delta\mu-2\,\mathbf{w}\cdot\boldsymbol{\ell})^3} \end{aligned} \tag{3.28}$$

which after simplification, exactly similar to the above, becomes

$$\begin{aligned} K &= -\frac{g}{2}\left(\frac{3}{4}\pi\rho T\,\mathrm{Re}\sum_{n=0}^{\infty}\frac{1}{\bar{\omega}_n^5}\right) \\ &= \frac{\gamma g}{2}. \end{aligned} \tag{3.29}$$

Note that we have kept only the constant term in K and not considered any momentum dependent terms to avoid higher order, irrelevant (in the RG sense) terms.

Finally, putting Π, J and K in Eq. (3.14), the GL free energy of a FFLO superconductor turns out to be

$$\begin{aligned}\Omega &= \sum_{\mathbf{k}}\left(\alpha+\frac{2\beta}{3}k^2+\frac{8\gamma}{15}k^4\right)|\phi_{\mathbf{k}}|^2+\frac{1}{2}\sum_{\mathbf{k_i}}\left(\beta+\frac{4\gamma}{9}\left(\mathbf{k}_1^2+\mathbf{k}_2^2+\mathbf{k}_3^2+\mathbf{k}_4^2\right.\right.\\ &+ \left.\left.\mathbf{k}_1\cdot\mathbf{k}_3+\mathbf{k}_2\cdot\mathbf{k}_4\right)\right)\phi_{\mathbf{k}_1}\phi^*_{\mathbf{k}_2}\phi_{\mathbf{k}_3}\phi^*_{\mathbf{k}_4}\delta_{\mathbf{k}_1-\mathbf{k}_2+\mathbf{k}_3-\mathbf{k}_4}+\frac{\gamma}{3}\sum_{\mathbf{k}_i}\phi_{\mathbf{k}_1}\phi^*_{\mathbf{k}_2}\phi_{\mathbf{k}_3}\phi^*_{\mathbf{k}_4}\\ &\phi_{\mathbf{k}_5}\phi^*_{\mathbf{k}_6}\delta_{\mathbf{k}_1-\mathbf{k}_2+\mathbf{k}_3-\mathbf{k}_4+\mathbf{k}_5-\mathbf{k}_6},\end{aligned} \tag{3.30}$$

This GL free energy of FFLO state can be rewritten in position space, after Fourier transformation, as

$$\begin{aligned}\Omega=\int d^dx \quad &\Big[\quad \alpha\phi^2+\frac{2\beta}{3}(\nabla\phi)^2+\frac{8\gamma}{15}(\nabla^2\phi)^2+\frac{\beta}{2}(\phi^2)^2-\frac{8\gamma}{9}\phi^2\phi\cdot(\nabla^2\phi)\\ &-\quad \frac{4\gamma}{9}\phi^2(\nabla\phi)^2+\frac{\gamma}{3}(\phi^2)^3\Big].\end{aligned} \tag{3.31}$$

To analyse the GL free energy thus obtained, in the next section we will discuss the physics of relevant multicritical points and relate them to it.

3.3 Lifshitz and Lifshitz-tricritical point

First of all, let us introduce the Lifshitz-tricritical class. From previous literature we find that, in a general study of tricritical and Lifshitz kind of behaviour, Aharony et al [99] started with the free energy in d-dimensions

$$\begin{aligned}\Omega=\frac{1}{2}\int d^dx \quad &\Big[\quad r\phi^2+\mu(\nabla_\alpha\phi)^2+(\nabla^2_\alpha\phi)^2+(\nabla_\beta\phi)^2+u\phi^4\\ &+\quad \lambda_1\phi^2\phi.(\nabla^2_\alpha\phi)+\lambda_2\phi^2(\nabla_\alpha\phi)^2+w\phi^6\Big],\end{aligned} \tag{3.32}$$

where α denotes an m-dimensional space with $m \leq d$ and subsequently $\nabla_\alpha = \sum_{i=1}^{m}\widehat{i}\nabla_i$, β denotes $(d-m)$ dimensional space with $\nabla_\beta=\sum_{i=1}^{d-m}\widehat{i}\nabla_i$. $\phi(\mathbf{x})$ is an n-

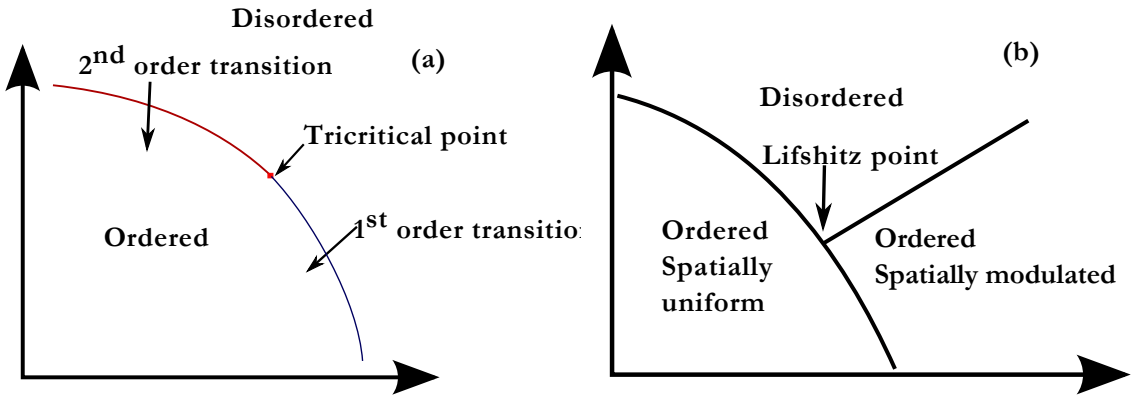

(a) Tricritical **(b)** Lifshitz

Figure 3.1 Schematic phase diagrams depicting a)tricritical and b)Lifshitz points.

component order parameter with $O(n)$ symmetry. Interestingly, comparing Eq. (3.32) and Eq. (3.31) we find that the FFLO state belong to the $(d-d)$, or isotropic, Lifshitz-tricritical class. In the previous FFLO literatures, this multicritical point had always been refereed as tricritical point [88,89], but we find it to be a Lifshitz tricritical point (LTP). We note that in Eq. (3.31) there is a fourth-order gradient term (quartic in momentum) which is quadratic in order parameter. This term is essential for the occurrence of a Lifshitz point. What is vital is that the coefficient of the gradient-square, quadratic ϕ term and quartic ϕ term in Eq. (3.31) changes sign at the same point, namely at $\beta = 0$. This is the LTP which we will take as the hallmark of the GL free energy of Eq. (3.31).

To better understand the LTP, let us now discuss it a bit. The system, described Eq. (3.32), can have several multicritical points. If we assume, in the spirit of mean-field theories, that the homogeneous state is the relevant one, then the derivatives in Eq. (3.32) are zero. For the usual second-order transition (critical point) the parameter r is temperature dependent and changes sign at the critical temperature.

If there is a second physical variable (e.g. He_3 concentration in the $He_3{-}He_4$ mixtures or the chemical potential imbalance as over here), the coefficient u of the quartic term is a function of that variable and a line of critical points can be generated. This line ends when it meets a line of first-order transitions which can occur for negative values of u. This end point is the tricritical point where a line of first-order and second-order transitions meet (see Fig. 3.1a). This simple picture of a homogeneous state is changed if the sign of the derivative squared term in the free energy is allowed to change. Then the homogeneous state is no longer the lowest energy one if this term is negative. To prevent instability, one needs a second derivative squared term of positive sign and thus a spatially modulated state is formed that minimizes the relevant part of the free energy. Hence depending on whether the derivative squared term is positive or negative, the thermodynamic state is spatially uniform or modulated. We have two transition lines once again - a line across which a disordered state becomes ordered and spatially uniform and another line across which a disordered state becomes ordered but spatially modulated. These two lines meet at the Lifshitz point (Fig. 3.1b). If it so happens that magically the tricritical and Lifshitz points occur simultaneously where r and u change sign at the same point, then one has a Lifshitz tricritical point.

3.4 Phase diagram

We now analyse Eq. (3.31) in two-dimensions to explore the mean-field phase diagram of FFLO state. For $\beta > 0$, the free energy minimum occurs at a spatially-constant ϕ, which we call ϕ_C. Then Eq. (3.31) reduces to $\Omega = V[\alpha\phi_C^2 + \beta\phi_C^4/2 + \gamma\phi_C^6/3]$. The term proportional to ϕ_C^6 is redundant (i.e. it is now a ϕ^4 model), and, for $\alpha < 0$ the system goes from the normal state ($\phi_C = 0$) to the homogeneous BCS superconducting state with zero center-of-mass momenta Cooper pairs.

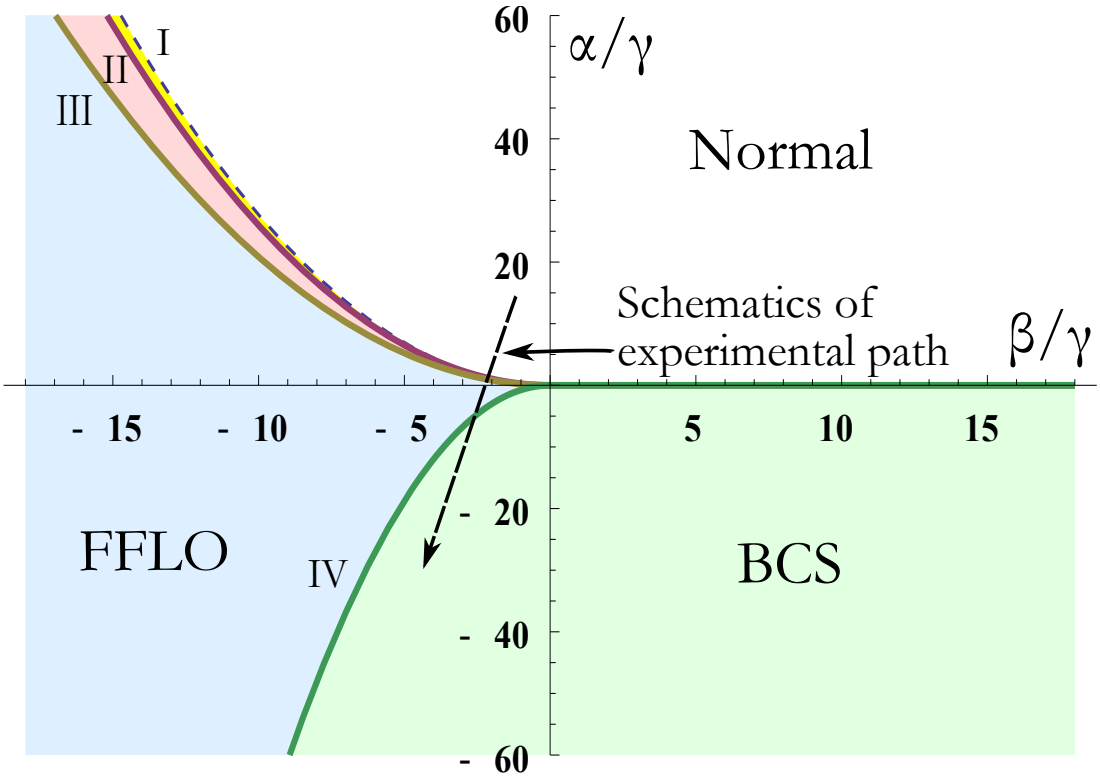

Figure 3.2 Phase diagram of a FFLO superconductor, at mean-field level, plotted as a function of α/γ and β/γ. Graphs I and II represents the metastable and first-order line, respectively. On curve III, the coefficient of the quadratic term in order parameter vanishes. On curve IV, the FFLO state goes to the BCS state as the wave number of the order parameter goes to 0.

For $\beta < 0$ BCS state no longer remains the minimum of GL free energy and we envisage a periodic variation of ϕ like $\phi(\mathbf{x}) = \phi_0 e^{i\mathbf{k}\cdot\mathbf{x}}$. With this $\phi(\mathbf{x})$, the GL free energy in Eq. (3.31) reduces to

$$\frac{\Omega}{V} = \left(\alpha - \frac{2|\beta|}{3}k^2 + \frac{8\gamma}{15}k^4\right)\phi_0^2 + \left(-\frac{|\beta|}{2} + \frac{4\gamma}{9}k^2\right)\phi_0^4 + \frac{\gamma}{3}\phi_0^6 \tag{3.33}$$

, where V is system's volume. Minimising this free energy with respect to $\mathbf{k}$ and substituting $\mathbf{k}$'s minimum value in above equation we obtain an effective ϕ^6 free

energy

$$\frac{\Omega}{V} = \left(\alpha - \frac{5\beta^2}{24\gamma}\right)\phi_0^2 - \frac{2|\beta|\phi_0^4}{9} + \frac{13\gamma\phi_0^6}{54}. \tag{3.34}$$

Since $\beta < 0$ in Eq. (3.34), the minimisation of Eq. (3.34) with respect to ϕ_0 gives a local minimum of Ω at a finite ϕ_0 when $\alpha = \alpha_1 = (259\beta^2)/(936\gamma)$, shown as graph I in Fig. 3.2. This signals the onset of a metastable state as the normal state with $\phi_0 = 0$ remains the global minima. When the system cooled further keeping β and γ fixed, a first-order transition occurs where the free energy at $\phi_0 \neq 0$ becomes the global minimum. This occurs at $\alpha = \alpha_2 = (27\beta^2)/(104\gamma)$, shown as graph II in Fig. 3.2. The FFLO state thus produced has a wave number which is given by $k_C^2 = 5\beta/8\gamma - 5\phi^2/12$, which clearly depends on the temperature and the magnetic field. At an even lower temperature of $\alpha = \alpha_3 = (5\beta^2)/(24\gamma)$, the coefficient of the quadratic ϕ_0-term in Eq. (3.34) vanishes (shown as graph III in Fig. 3.2). A further lowering of the temperature causes the wave number of the FFLO order parameter to decrease and at the boundary IV this wave number goes to 0 signalling the end of the FFLO phase. The system thereafter makes a transition to the standard BCS phase. Thus in our scheme of things, FFLO state exists between boundaries II and IV and these are the two places where a specific heat anomaly will be seen. This is what is seen in the experiment of Lortz et al [65].

3.5 Calculation of specific heat

With this phase diagram available, we are now ready to find the behaviour of specific heat near the first-order transition. Above the first-order transition temperature(α_2), the mean-field specific heat is identically zero. To calculate its value above the first-order line, we consider Gaussian fluctuations around the mean-field value and calcu-

late the partition function

$$Z = \int \mathcal{D}\phi \exp[-\Omega_g / k_B T_C] \tag{3.35}$$

in which

$$\Omega_g = \sum_{\mathbf{k}} \big(\alpha - \frac{2|\beta|}{3}k^2 + \frac{8\gamma}{15}k^4\big)|\phi_{\mathbf{k}}|^2 \tag{3.36}$$

is the Gaussian free energy. We have considered $\beta < 0$ as we are below the metastable line. We minimise this free energy with respect to $\mathbf{k}$ and write $\mathbf{k} = \mathbf{k}_C + \mathbf{l}$ where $k_C^2 = 5|\beta|/8\gamma$. The thermodynamic free energy per unit volume is given by $F = -k_B T_C \ln Z$. The Gaussian specific heat per unit volume, the second derivative of F with respect to α, comes out to be

$$C_g = \frac{3\sqrt{3}k_B}{128\pi}|\beta|^{-3/2}(\alpha - 5\beta^2/24\gamma)^{-1/2}. \tag{3.37}$$

The Gaussian specific heat, evaluated at the first-order temperature, is plotted as curve (1) in Fig. 3.3a. Here we point out that Konschelle et al [101] got an anomalous exponent for C_g as they considered fluctuations around $\mathbf{k}_C$ in the radial direction alone. We further observe that inclusion of the higher order ϕ terms will lead to a substantial increase in the rate of divergence of C_g as shown by Aharony et al [99] who evaluated the first-order correction to the specific heat using renormalization group analysis. However, for temperatures above the first-order temperature, which is greater than the temperature at which C_g diverges, the Gaussian specific heat accurately represents the fluctuation specific heat. To find the specific heat of the system below the first-order temperature, we evaluate the mean-field specific heat. This can be calculated by taking the double derivative of the mean-field GL free energy of Eq. (3.34) with respect to α, the temperature parameter. The mean-field specific heat per unit volume is given by

$$C_{mf} = 18k_B(259\beta^2 - 936\alpha\gamma)^{-1/2}. \tag{3.38}$$

We have plotted C_{mf} at the first-order temperature as curve (2) in Fig. 3.3a.

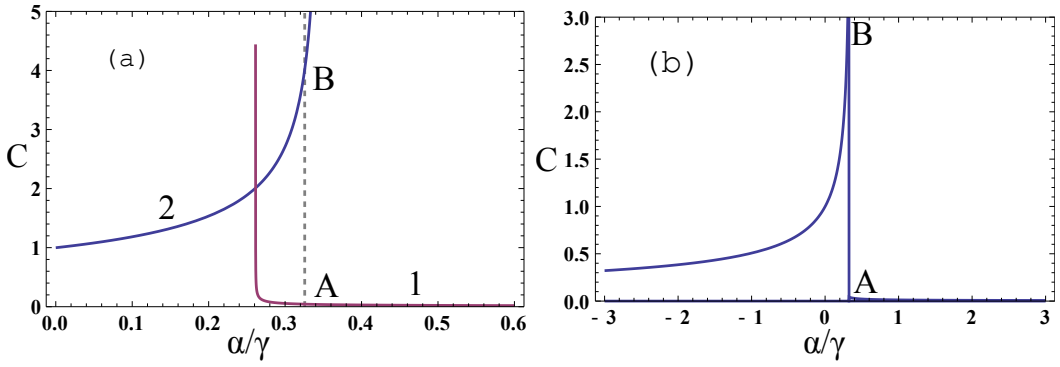

(a) From theory **(b)** From theory (zoomed)

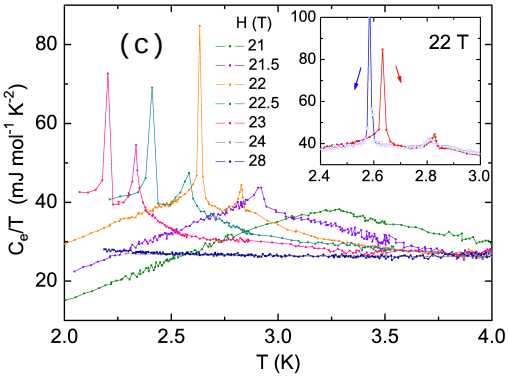

(c) From experiment

Figure 3.3 Plot of the specific heat as a function of the scaled temperature. As the system is cooled from the normal state, it exhibits Gaussian specific heat, plotted as curve (1) in Fig. a. At the first-order transition temperature, the specific heat jumps from point A to B and starts following the mean-field specific heat, plotted as curve (2). Fig. b focusses only on the jump in specific heat . The experimental plot of specific heat of the layered organic superconductor, as obtained by Lortz et al [65], showing the anomalous jump of the specific heat is shown in Fig. c.

3.6 Explanation of experimental findings

Let us now discuss how this model can describe the findings by Lortz et al [65]. When one cools the imbalanced fermionic system from the normal state, one measures the Gaussian specific heat. As the system cools to the first-order transition temperature, the specific heat jumps to its mean-field value and FFLO state appears. If one cools the system further, then at a sufficiently low temperature the system goes to the BCS state as the wave number of the FFLO state becomes 0 and subsequently the specific heat jumps to the BCS mean-field value signalling this transition. We have shown a schematic experimental path in Fig. 3.2, which, we argue, is the path taken in the experiment of Lortz et al showing two jumps in the specific heat. Considering the experimental data for specific heat jump at a magnetic field, applied parallel to the superconducting layers, of 22 T, we find $(\alpha\beta)^{1/2} = 0.008$. The jump of the specific heat is plotted in Fig. 3.3b and we have also shown the experimental specific heat diagram from Lortz et al in Fig. 3.3c. To provide a more quantitative relation between our theory and Lortz's experiment we have done a study on the relation between the size of the specific heat's jump and the magnetic field. In experiment, it was found that the jump size increased as the magnetic field was increased. In our theoretical model, we have checked and found that the size of specific heat jump increases with increase in the chemical potential imbalance which, being directly proportional to the applied magnetic field, is equivalent to the applied magnetic field. The reader is referred to Fig. 3.4 for the theoretical and experimental plots. Thus we have shown that the static analysis of the GL free energy provides the reason for the jump in specific heat.

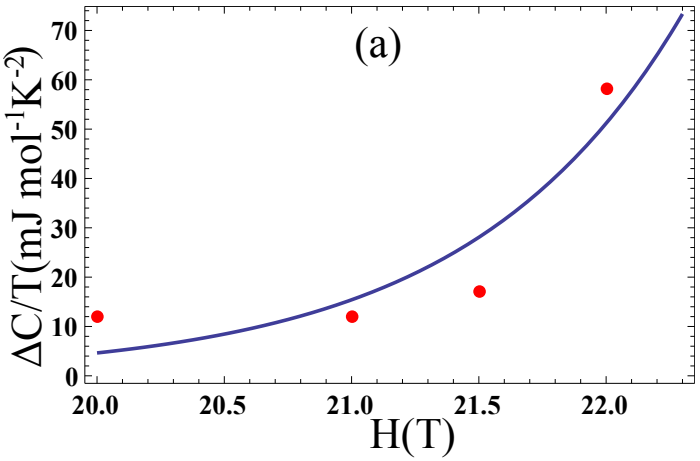

(a) From experiment

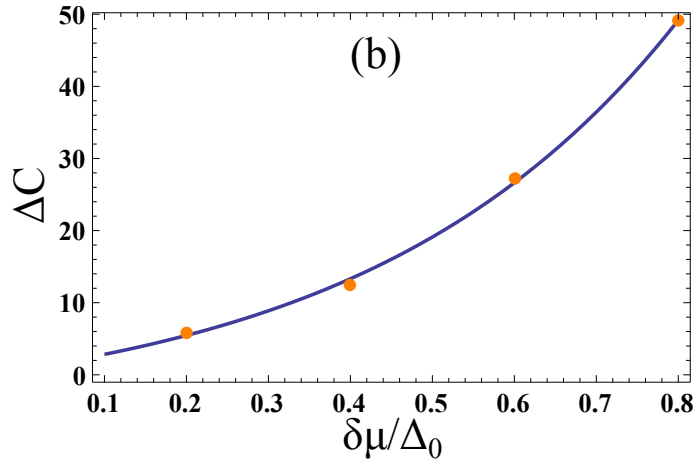

(b) From theory

Figure 3.4 Fig. a shows that the size of jump in specific heat, as the system enters into FFLO state, increases with the increase in applied magnetic field. In Fig. b, we have shown that our theory also predicts a similar increase in the specific heat as the applied magnetic field and thus the imbalance in chemical potential increase. The fits are provided as guides to the eyes.

3.7 Dynamical study of the free energy

Now to find a way for pinpointing the region in the phase diagram where one will find the jump in specific heat in an experiment, we have studied the dynamics of

this system near LTP using TDGL formalism. This study has also been encouraged by a very recent study by Sodemann et al [102] who showed that finite-momentum superfluid state occupies a large area in the phase diagram of an imbalanced fermionic system just following a quench from the normal to the superconducting state than in the equilibrium phase diagram of the same system. In our study, we look for the growth of FFLO phase following a quench. The TDGL for this system can be written as $\partial\phi_k/\partial t = -\Gamma(\delta\Omega/\delta\phi_{-k})$, in Fourier space where Ω is the GL free energy in Eq. (3.30). The quantity of experimental relevance is the dynamical correlation function or the structure factor $S(\mathbf{k},t) = \langle\phi_{\mathbf{k}}(t)\phi_{-\mathbf{k}}(t)\rangle$. To begin with, the dynamics of $\phi_{\mathbf{k}}$ is governed by

$$\begin{aligned}
\frac{\partial\phi_{\mathbf{k}}}{\partial t} &= -\Gamma\frac{\partial\Omega}{\partial\phi_{-\mathbf{k}}} \\
&= -2\Gamma\left(\alpha + \frac{2\beta}{3}k^2 + \frac{8\gamma}{15}k^4\right)\phi_{\mathbf{k}} - 2\beta\Gamma\sum_{\mathbf{k_1},\mathbf{k_2}}\phi_{\mathbf{k_1}}\phi_{\mathbf{k_2}}\phi_{\mathbf{k}-\mathbf{k_1}-\mathbf{k_2}} \\
&- \frac{8\gamma\Gamma}{9}\sum_{\mathbf{k_1},\mathbf{k_2}}(2k^2 + k_1^2 + 2k_2^2 + \mathbf{k_1}\cdot\mathbf{k_2} - \mathbf{k}\cdot\mathbf{k_1} - 3\mathbf{k}\cdot\mathbf{k_2})\phi_{\mathbf{k_1}}\phi_{\mathbf{k_2}}\phi_{\mathbf{k}-\mathbf{k_1}-\mathbf{k_2}} \\
&- 2\gamma\Gamma\sum_{\mathbf{k_1},\mathbf{k_2},\mathbf{k_3},\mathbf{k_4}}\phi_{\mathbf{k_1}}\phi_{\mathbf{k_2}}\phi_{\mathbf{k_3}}\phi_{\mathbf{k_4}}\phi_{\mathbf{k}-\mathbf{k_1}-\mathbf{k_2}-\mathbf{k_3}-\mathbf{k_4}} \qquad (3.39)
\end{aligned}$$

The structure factor, subsequently, evolves according to

$$\begin{aligned}
&\frac{\partial S_{\mathbf{k}}}{\partial t} = -4\Gamma\left(\alpha + \frac{2\beta}{3}k^2 + \frac{8\gamma}{15}k^4\right)S_{\mathbf{k}} - 4\beta\Gamma\left\langle\sum_{\mathbf{k_1},\mathbf{k_2}}\phi_{\mathbf{k_1}}\phi_{\mathbf{k_2}}\phi_{\mathbf{k}-\mathbf{k_1}-\mathbf{k_2}}\phi_{-\mathbf{k}}\right\rangle \\
&-4\gamma\Gamma\left\langle\sum_{\mathbf{k_1},\mathbf{k_2},\mathbf{k_3},\mathbf{k_4}}\phi_{\mathbf{k_1}}\phi_{\mathbf{k_2}}\phi_{\mathbf{k_3}}\phi_{\mathbf{k_4}}\phi_{\mathbf{k}-\mathbf{k_1}-\mathbf{k_2}-\mathbf{k_3}-\mathbf{k_4}}\phi_{-\mathbf{k}}\right\rangle \\
&-\frac{16\gamma\Gamma}{9}\left\langle\sum_{\mathbf{k_1},\mathbf{k_2}}(2k^2 + k_1^2 + 2k_2^2 + \mathbf{k_1}\cdot\mathbf{k_2} - \mathbf{k}\cdot\mathbf{k_1} - 3\mathbf{k}\cdot\mathbf{k_2})\phi_{\mathbf{k_1}}\phi_{\mathbf{k_2}}\phi_{\mathbf{k}-\mathbf{k_1}-\mathbf{k_2}}\phi_{-\mathbf{k}}\right\rangle. \\
&\qquad (3.40)
\end{aligned}$$

To make any progress, we require to deal with the quartic and sextic correlations. As a first approximation this is done in the Hartree approximation, in which the

correlation functions factor. Implementing this we get

$$\sum_{\mathbf{k_1},\mathbf{k_2}} \left\langle \phi_{\mathbf{k_1}} \phi_{\mathbf{k_2}} \phi_{\mathbf{k}-\mathbf{k_1}-\mathbf{k_2}} \phi_{-\mathbf{k}} \right\rangle = 3 \sum_{\mathbf{p}} S_{\mathbf{p}}(t) S_{\mathbf{k}}(t) \tag{3.41}$$

and

$$\left\langle \sum_{\mathbf{k_1},\mathbf{k_2},\mathbf{k_3},\mathbf{k_4}} \phi_{\mathbf{k_1}} \phi_{\mathbf{k_2}} \phi_{\mathbf{k_3}} \phi_{\mathbf{k_4}} \phi_{\mathbf{k}-\mathbf{k_1}-\mathbf{k_2}-\mathbf{k_3}-\mathbf{k_4}} \phi_{-\mathbf{k}} \right\rangle = 15 \left(\sum_{\mathbf{p}} S_{\mathbf{p}}(t) \right)^2 S_{\mathbf{k}}(t) \tag{3.42}$$

Implementing this on Eq. (3.40), we arrive at

$$\begin{aligned} \frac{\partial S_{\mathbf{k}}}{\partial t} = -4\Gamma \quad \Bigg[& \quad \alpha + \frac{2\beta}{3} k^2 + \frac{8\gamma}{15} k^4 + 3\beta \sum_{\mathbf{p}} S_{\mathbf{p}} + \frac{8\gamma}{9} k^2 \sum_{\mathbf{p}} S_{\mathbf{p}} \\ & + \quad \frac{8\gamma}{9} \sum_{\mathbf{p}} p^2 S_{\mathbf{p}} + 15\gamma \Big(\sum_{\mathbf{p}} S_{\mathbf{p}} \Big)^2 \Bigg] S_{\mathbf{k}}. \end{aligned} \tag{3.43}$$

At very short times, when $S_{\mathbf{k}}$ is small, we can write the solution to the above equation in the region $\beta < 0$ as

$$S_{\mathbf{k}}(t) = S_{\mathbf{k}}(0) e^{-4\Gamma\left(\alpha + \frac{2\beta}{3} k^2 + \frac{8\gamma}{15} k^4\right) t}. \tag{3.44}$$

This results in an interesting consequence: if $\alpha > 5\beta^2/24\gamma$ and we quench in the region between line II and III in the phase diagram (Fig. 3.2) all modes of the order parameter decay quickly. However if $\alpha < 5\beta^2/24\gamma$, there exist a band of wave numbers around a critical wave number ($k_C = \sqrt{(5|\beta|/8\gamma)}$) for which the structure factor grows. Thus the decay or growth of the structure factor in short time limit actually indicates the existence of the line III in the phase diagram (Fig. 3.2), which static analysis cannot probe.

We now claim that the wave number $k = k_C$ can be found experimentally if one quenches the system beyond the first order line, i.e. beyond the line point where the specific heat had a sudden change and look for the long-time dynamics. To look for the long-time dynamics we work, as before, for $\beta < 0$ and expand the wave number

around $\mathbf{k}_C$, i.e. write $\mathbf{k} = \mathbf{k}_C + \mathbf{l}$. Restricting to terms quadratic in '$\mathbf{l}$' we can rewrite Eq. (3.43) as

$$\frac{\partial S_{\mathbf{k}}}{\partial t} = -\frac{16\Gamma\beta l^2}{3} S_{\mathbf{k}} - f(t) S_{\mathbf{k}} \tag{3.45}$$

where

$$f(t) = -4\Gamma\Big[\alpha - \frac{5\beta^2}{24\gamma} + \Big(3\beta + \frac{8\gamma}{9}k^2\Big)\sum_{\mathbf{p}} S_{\mathbf{p}} + \frac{8\gamma}{9}\sum_{\mathbf{p}} p^2 S_{\mathbf{p}} + 15\gamma\Big(\sum_{\mathbf{p}} S_{\mathbf{p}}\Big)^2\Big] \tag{3.46}$$

This allows us to write the solution of Eq. (3.45) as

$$S_{\mathbf{k}}(t) = \Delta \exp\Big[-\frac{16\Gamma\beta l^2}{3} t - g(t)\Big] \tag{3.47}$$

where $g(t) = \int_0^t dt' f(t')$. If one now demand, as one does in this kind of self-consistent calculation [103, 104], that $\sum_{\mathbf{p}} S_{\mathbf{p}}$ goes to some constant value as $t \to \infty$, thus obtaining the ordered state; then for $t \to \infty$ one can neglect the sub-leading $\sum_{\mathbf{p}} p^2 S_{\mathbf{p}}$ term, and, the final result for the structure factor comes out to be

$$S_{\mathbf{k}}(t) = \Delta t^{3/2} \exp\Big[-\frac{8\gamma}{15}(k^2 - k_C^2) t\Big] \tag{3.48}$$

This result shows that at long time after the quench $S_{\mathbf{k}}(t) \to 0$ for all wave numbers expect $\mathbf{k} = \mathbf{k}_C$. So determination of the parameter k_C^2 actually fixes the ratio β/γ of the phenomenological model of Eq. (3.30).

3.8 Summary and discussion

In conclusion our analysis explains the specific heat data, the first-order transition and the exact realization of the phase diagram of the FFLO state in 2D organic superconductors. In particular, we have studied the FFLO phase diagram using the phenomenological GL free energy and found that the phase diagram contains a LTP. We have calculated the specific heat and found that it jumps near the first-order line

in the phase diagram as we lower the temperature, as also found in an experiment by Lortz et al [65]. By doing a dynamical analysis of the GL free energy, we suggest a way to explore the portion of the phase diagram where one should look for the jump. In passing, we note that for a complete explanation of the FFLO state some more material-dependent inputs like the exact shape of the Fermi surface, the mean free path and other parameters are needed, in addition to our phenomenological model. A possible extension of our work can be performing the dynamical analysis beyond the Hartree approximation and exploring the elusive FFLO state further.

Chapter 4

Holographic entanglement entropy and imbalanced superconductors

4.1 Introduction

Holography is a remarkable concept that plays vital role to understand many features in modern physics– starting from black holes and cosmology to AdS/CFT correspondence. Historically it was first realized through the expression of black hole entropy [105, 106]

$$S_{BH} = \frac{\text{Area}(\Sigma_H)}{4G_N} \tag{4.1}$$

which was found surprisingly proportional to the horizon area and not the volume. It motivates one to think that the bulk degrees of freedom somehow "holographically" mapped to the surface/horizon degrees of freedom which results this non-extensive behaviour in entropy. Later on this enabled 't Hooft, Susskind and others [107–110] to explain our Universe using the concept of holography. Most recent additions to this list are AdS/CFT correspondence and entanglement entropy.

4.1.1 AdS/CFT correspondence

AdS/CFT correspondence, first conjectured by Maldacena [111], is a realization of much discussed proposition of 't Hooft [112] on the large N limit of strong interactions. AdS/CFT correspondence states that a supergravity theory in $AdS_5 \times S^5$ is a "dual" description of strongly coupled $\mathcal{N} = 4$, $SU(N)$ SYM theory "residing" in its boundary in the limit of $N \to \infty$. Here S^5 is compactified to a radius $L >> l_s$ (l_s= string length) which is also the radius of curvature of AdS spacetime. Therefore effectively a five dimensional gravity theory is "holographically" reduced to a four dimensional conformal field theory. This "duality" in two theories was quantified by Witten [113], by identifying the bulk field with boundary operator and n point correlation functions in terms of derivatives of the gravitational partition function with respect to the boundary value of that field. In support of this yet unproven AdS-CFT correspondence, there exists many direct and indirect evidences, for example–(i) the isometry group $SO(4,2)$ of AdS_5 is isomorphic to the conformal group of the SYM theory, (ii) matching of correlation functions calculated separately from CFT and that using AdS/CFT tool and many others (for more see reviews [114]- [115]), which make it robust. It is true that the exact reason/s why such two apparently different theories should behave so cohesively is/are not known, but the role of holography is undeniable, and therefore it needs further attention. The major applications of this correspondence can be broadly classified in two parts: one which are in the context of QCD (for a review see [116]) and the other in the context of condensed matter physics [67, 71].

4.1.2 Holographic entanglement entropy (HEE)

The role of holography in the much focussed issue of entanglement entropy has been recently highlighted by Ryu and Takayanagi [117, 118]. If a system, described by certain quantum field theory or some quantum many body theory, is divided into two parts, say A and B, then entanglement entropy S_A of the subsystem A is a non-local quantity which measures how the above systems are correlated, quantum mechanically, with each other. In defining S_A one traces out the degrees of freedom of the space-like submanifold B which is not accessible to an observer in A. Anyone familiar with the concept of black hole entropy would find this definition very much analogous to the case where an observer outside the black hole event horizon has no access to the information inside. Indeed this is one of the motivation for the authors of [117,118] to *heuristically* propose an "holographic" formula of entanglement entropy, given by

$$S_A = \frac{\text{Area}(\gamma_A)}{4G_N} \tag{4.2}$$

where γ_A is the d dimensional surface whose $d-1$ dimensional boundary ∂_{γ_A} matches with the boundary ∂_A of the field theory subsystem A (*see* Fig. 4.1). Of course the choice for such a surface is not unique. In this context it is suggested that this surface, among various choices, should be the *minimal*. This minimal surface is found by extremizing the area functional and finding out the solution (in case there are more than one) whose area takes the minimum value.

At the present status the HEE formula (4.2) is not conclusively proven[1]. Nevertheless there is a list of evidences which bolsters the robustness of this formula. One direct evidence comes from the AdS_3/CFT_2 context where the CFT result of the entanglement entropy $S_A = \frac{c}{3}\log\frac{l}{a}$, matches with the holographic calculation, in

[1]Refer to [119] for an attempt and others [120, 121] for more details.

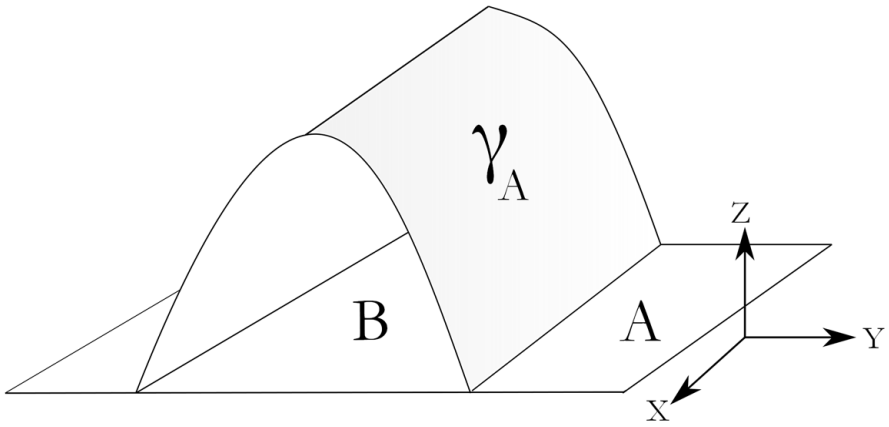

Figure 4.1 Schematic diagram of the computational scheme of holographic entanglement entropy via AdS/CFT. The field theory system "resides" on the planar portion, whereas, the minimal (entangled) surface γ_A is extended inside the bulk (z axis) towards the horizon (not shown in the figure).

which l is the width of the subsystem A and $c = \frac{3R}{2G_N}$ relates the central charge c with the radius of curvature R of the AdS_3 spacetime. Although this evidence has not been explicitly seen in higher dimensional cases (AdS_{d+1}/CFT_d with $d > 2$), there are more compelling arguments which put confidence on (4.2) (*for details see reviews* [122, 123] *and references therein*). The major usefulness of the HEE is the same as the basic principle of AdS/ CFT: overcoming the computational difficulties of complex many body field theoretic calculations in terms of much more simpler classical gravity calculations.

4.1.3 HEE for holographic superconductors

Our work, described in this chapter[2], is motivated by a recent study by Albash and Johnson [124, 125], where it is argued that HEE might be an useful physical quantity for characterizing holographic superconductors. They found that the finite part of the HEE (S_f) of superconducting and non-superconducting phases follow a pattern which enables one to identify the phase of a system. For a given system size and for all temperatures below the critical value T_c, S_f takes a lower value for the superconducting phase compared to its value for the corresponding non-superconducting (black hole) phase. Whereas for temperature higher than T_c, where no superconducting state appears, S_f only exist for the latter phase. The reason behind the smaller value of HEE for the superconducting state is explained in terms of number of the degrees of freedom that the system possesses. This number is higher in the black hole phase but as the superconductor forms some of them are condensed and results into a lower HEE. Further works in this direction are also reported in [126]- [127]. It should also be mentioned that apart from the finite value of HEE given by S_f there is also a diverging part. However, such a divergence is not the characteristic of the holographic calculation only, it also appears in the continuum limit of the conformal field theory calculations. One can avoid such diverging terms by introducing a UV cut off through the introduction of a lattice spacing in the expression of entanglement entropy. In the holographic calculation, the divergences can be avoided if the boundary of the minimal surface is chosen slightly away from the asymptotic infinity by choosing the appropriate limit of the radial coordinate.

[2]The work reported here is based on the paper "Holographic entanglement entropy in imbalanced superconductors", Arghya Dutta and Sujoy K. Modak, **JHEP**, 01, (2014), 136.

4.1.4 Our work: HEE for imbalanced holographic superconductor

In this chapter we explore the behaviour of HEE in an *imbalanced mixture* of two fermionic systems with a mismatch in their chemical potentials [74]. One motivation of choosing the imbalanced system is that these are quite interesting in the condensed matter framework. This is discussed in more detail in the introduction (See section 1.2.4). Our aim is to compute the HEE for two phases (black hole and superconducting phases) and compare their numerical values as a function of the strip size. The gravitational system is considered to have the backreaction term. We use numerical shooting method to find the hairy black hole solution for two different values of chemical mismatch 0.01 and 0.02 and compare the results for HEE with the black hole phase with same chemical potential and temperature. For both cases we find that HEE for the superconducting phase stay below the black hole phase. On the other hand the effect of the imbalance on HEE is exactly opposite for the superconducting phase than the black hole phase. While HEE increases with the increase in imbalance parameter for black holes it decreases when superconducting state forms. This demands a more careful interpretation whether HEE can always be used for identifying the preferable state or not. The reason being one expects that for increasing chemical imbalance the superconducting state is hard to achieve and at a certain larger value this state disappears. But from our study it appears that the gap of HEE between the black hole and superconductor only increases. Superconducting state is more and more stable with the increase in chemical imbalance if one solely relies on HEE. And in that way one never gets rid of the superconducting state. This contradicts the usual expectations.

4.2 Holography and imbalanced superconductor

Recently there has been a lot of effort [73, 74, 128–131] to understand the imbalanced superconducting systems using holography and AdS/CMT. Generally, the bulk gravitational Lagrangian which holographically describe an imbalanced superconductor is given by

$$\mathcal{L} = \frac{\sqrt{-g}}{2k_4^2}\left(R + \frac{6}{L^2} - \frac{1}{4}F_{ab}F^{ab} - -\frac{1}{4}Y_{ab}Y^{ab} - V(|\phi|) - |\partial\phi - iqA\phi|^2\right) \tag{4.3}$$

which is comprised of the AdS gravity with $\Lambda = -\frac{6}{L^2}$, two $U(1)$ gauge fields with field strengths

$$F = dA, \qquad Y = dB, \tag{4.4}$$

and one scalar field (ϕ) with potential

$$V(|\phi|) = m^2\phi^\dagger\phi \tag{4.5}$$

which is charged under $U_A(1)$ but uncharged with respect to the other.

As known from the AdS/CFT correspondence mass of the above bulk scalar field dictates the conformal dimension (Δ) of the dual field in the following manner

$$\Delta(\Delta - 3) = m^2L^2. \tag{4.6}$$

This relation is particularly helpful to capture the physics of an field theory operator with a conformal dimension of interest. For example to describe a Cooper pair type condensate which has $\Delta = 2$, one fixes the mass of the bulk scalar field to be $m^2 = -\frac{2}{L^2}$. Note that this choice does not violate the Brietelhoner-Freedman bound which for this case is $m^2 \geq -\frac{9}{4L^2}$. Since our interest lies in this theoretical aspect, in this work, we will fix the above mass value for the bulk scalar field in all our computations. For completeness it should be mentioned that other than mass, the scalar field also

has a charge q, and different values of charge lead to different physical properties in the dual field theory.

The above description of the gravitational system has the minimal ingredients needed to describe the superconductivity in the imbalanced systems. Starting from the equations of motion which include Einstein equations, Maxwell equations and a scalar field equation, one looks for the cases where the scalar field is zero and non-zero. The vanishing of the scalar field gives a normal Reissner-Nordström black hole phase. On the other hand, if one finds a non-zero scalar field it is understood that a condensate has been formed in the dual field theory. Of course this situation has a serious contradiction with the black hole no-hair theorem that supports the vanishing scalar field, but the fact of getting non-zero scalar field in the context of holographic superconductors hints that one needs to re-examine the no-hair theorem itself [132,133]. The above statement is true for any holographic superconductor. For the imbalanced case, with two $U(1)$ gauge fields with unequal chemical potential, we have the following additional advantage.

In imbalanced superconducting systems Cooper pair forms between two fermionic species with unequal chemical potentials (say μ_1 and μ_2). Now to capture this behaviour in the dual gravitational theory, one needs two $U(1)$ bulk fields (say $U_A(1)$ and $U_B(1)$) with field strengths A_a which accounts total chemical potential $2\mu = \mu_1 + \mu_2$ and B_a which accounts the mismatch $2\delta\mu(= \beta\mu) = \mu_1 - \mu_2$ of those fermionic species in boundary theory.

With these preliminaries we now move to the next sections to deal with the equations of motion and to compute the HEE separately for black hole and superconducting phases.

4.3 Equations of motion

Extemizing the Lagrangian (4.3) with respect to various fields one has the following set of equations:

Einstein equation,

$$G_{ab} + \frac{1}{2}\Lambda g_{ab} = -\frac{1}{2}T_{ab} \tag{4.7}$$

where the energy-momentum tensor of the matter field is defined as $T_{ab} = \frac{2}{\sqrt{-g}}\frac{\delta \mathcal{L}_{matter}}{\delta g^{ab}}$.

Maxwell equations for A_a and B_a fields reads

$$\frac{1}{\sqrt{-g}}\partial_a(\sqrt{-g}g^{ab}g^{cd}F_{bc}) = iqg^{dc}[\phi^\dagger(\partial_c\phi - iqA_c\phi) - \phi(\partial_c\phi^\dagger + iqA_c\phi^\dagger)] \tag{4.8}$$

$$\frac{1}{\sqrt{-g}}\partial_a(\sqrt{-g}g^{ab}g^{cd}Y_{bc}) = 0 \tag{4.9}$$

where the scalar/gauge coupling takes place only in $U_A(1)$ sector.

In addition there is also a scalar field equation given by

$$\frac{1}{\sqrt{-g}}\partial_a[\sqrt{-g}g^{ab}(\partial_b\phi - iqA_b\phi)] + iqg^{ab}A_b(\partial_a\phi - iqA_a\phi) + \frac{\phi}{2|\phi|}V'(|\phi|) = 0 \tag{4.10}$$

In order to proceed further we consider the following background metric

$$ds^2 = -g(r)e^{-\chi(r)}dt^2 + \frac{r^2}{L^2}(dx^2 + dy^2) + \frac{dr^2}{g(r)} \tag{4.11}$$

where $\chi(r)$ accounts for the backreaction due to matter fields. For a case where backreaction is negligible one sets $\chi = 0$. For all matter fields, the ansatz is assumed to be homogeneous

$$\phi = \phi(r), \qquad A_a dx^a = \psi(r)dt, \qquad B_a dx^a = v(r)dt \tag{4.12}$$

Now one finally unwinds all field equations by substituting the ansatz. The final set of equations now has two independent Einstein equations

$$\frac{1}{2}\phi'^2 + \frac{e^\chi(\psi'^2 + v'^2)}{4g} + \frac{g'}{gr} + \frac{1}{r^2} - \frac{3}{gL^2} + \frac{V(\phi)}{2g} + \frac{e^\chi q^2\phi^2\psi^2}{2g^2} = 0 \tag{4.13}$$

$$\chi' + r(\phi'^2 + \frac{e^\chi q^2\phi^2\psi^2}{g^2}) = 0 \tag{4.14}$$

two Maxwell equations for ψ and v fields

$$\psi'' + \psi'(\frac{2}{r} + \frac{\chi'}{2}) - \frac{2q^2\phi^2}{g}\psi = 0 \tag{4.15}$$

$$v'' + v'(\frac{2}{r} + \frac{\chi'}{2}) = 0 \tag{4.16}$$

and a scalar field equation

$$\phi'' + \phi'(\frac{g'}{g} + \frac{2}{r} - \frac{\chi'}{2}) - \frac{V'(\phi)}{2g} + \frac{e^{\chi}q^2\phi^2\psi^2}{2g^2} = 0. \tag{4.17}$$

In the remaining part of our work we will look for the simultaneous solution of the above set of equations to compute the HEE. From now on we set $2k_4^2 = 1,\ L = 1$.

4.4 HEE for the normal (black hole) phase with varying β

At high temperature (above T_c), when no superconductivity appears, one has a vanishing bulk scalar field. For such a case the right hand side of the Maxwell equation (Eq. (4.8)) vanishes and the resulting solution of the set of field equations is a doubly charged Reissner-Nordström black hole given by the metric

$$ds^2 = -f(r)dt^2 + \frac{dr^2}{f(r)} + r^2(dx^2 + dy^2), \tag{4.18}$$

$$f(r) = r^2(1 - \frac{r_H^3}{r^3}) + \frac{\mu^2 r_H^2}{4r^2}(1 - \frac{r}{r_H})(1 + \beta^2) \tag{4.19}$$

$$\beta = \frac{\delta\mu}{\mu} \tag{4.20}$$

where the gauge fields are

$$\psi(r) = \mu(1 - \frac{r_H}{r}) = \mu - \frac{\rho}{r}, \tag{4.21}$$

$$v(r) = \delta\mu(1 - \frac{r_H}{r}) = \delta\mu - \frac{\delta\rho}{r}. \tag{4.22}$$

Hawking temperature of this RN-AdS spacetime is given by

$$T_{bh} = \frac{r_H}{16\pi}[12 - \tilde{\mu}^2(1+\beta^2)], \tag{4.23}$$

$$\tilde{\mu} = \frac{\mu}{r_H}. \tag{4.24}$$

To compute HEE we change the radial coordinate from r to $z = \frac{r_H}{r}$. This redefinition has some computational convenience. In the $t,\ z,\ x,\ y$ system the metric looks like

$$ds^2 = -r_H^2 e^{-\chi} g(z) dt^2 + \frac{dz^2}{z^4 g(z)} + \frac{r_H^2}{z^2}(dx^2 + dy^2), \tag{4.25}$$

$$g(z) = \frac{1}{z^2} - [1 + \frac{\tilde{\mu}^2}{4}(1+\beta^2)]z + z^2\frac{\tilde{\mu}^2}{4}(1+\beta^2). \tag{4.26}$$

$$\tag{4.27}$$

The HEE expression (4.2) now simplifies to

$$S_E = \frac{1}{4}\int_0^{L_y}\int_{-l/2}^{l/2}\sqrt{h}\ dxdy \tag{4.28}$$

$$= \frac{L_y r_H}{4}\int_{-l/2}^{l/2}\frac{1}{z^2}\left(r_H^2 + \frac{z'^2}{z^2 g(z)}\right)^{1/2} dx \tag{4.29}$$

where 'h' is the determinant of the induced metric of the codimension 2 hypersurface and in the second equality prime denotes derivative with respect to x. Eq. (4.29) also tells us that the system is equivalent to one defined by the Lagrangian $L = \frac{1}{r_H z^2}\left(r_H^2 + \frac{z'^2}{z^2 f(z)}\right)^{1/2}$. In order to takes into account that the surface is minimal, we extremize the Lagrangian. This extremization problem has a constant of motion which is nothing but the canonical Hamiltonian. In this way we obtain a measure of how the entangling surface is extended within the bulk (towards the horizon) and gives an infrared cut-off (z_0) on the integrating variable, which is given by

$$\frac{1}{z_0^2} = \frac{r_H}{z^2}\frac{1}{\sqrt{r_H^2 + \frac{z'^2}{z^2 g(z)}}} \tag{4.30}$$

Then converting the integrating variable from x to z the final expression of HEE reads as

$$S_E = \frac{L_y r_H^2}{2} \int_\epsilon^{z_0} \frac{z_0^2}{z^3} \frac{1}{\sqrt{(z_0^4 - z^4) g(z)}} \tag{4.31}$$

$$= S_f + S_{div}, \tag{4.32}$$

where S_f and S_{div} parts denote the finite and diverging part of the entanglement entropy as discussed earlier.

On the other hand the width of the subsystem 'A' is expressed as

$$\frac{l}{2} = \int_0^{l/2} dx \tag{4.33}$$

$$= \frac{1}{r_H} \int_\epsilon^{z_0} \frac{z dz}{\sqrt{g(z)(z_0^4 - z^4)}} \tag{4.34}$$

So finally to explore the behaviour of the HEE, one now needs to evaluate the expressions (4.31) and (4.34). For this we need to find the metric function $g(z)$ for different cases - namely for the AdS-RN black hole and the imbalanced superconductor, set the UV cut-off ϵ to a small value and consider z_0 near to the horizon. We note that by changing z_0 it is possible to study the behaviour of S_f as a function of the strip width l.

Doing this is easy for the black hole phase since we know the black hole metric explicitly. In Fig. 4.2 we show the variation of HEE with respect to the strip width for a fixed temperature $T_{bh} = 0.13$ and for different values of the imbalance parameter β. The larger l corresponds to the infra-red limit [124]. In addition to conforming the earlier results [124], from this set of plots we find that if one keeps the system-size as well as temperature constant, HEE for RN-AdS phase increases with the increase in chemical potential imbalance β. This has the following important physical consequence: if one considers HEE as a measure of the number of degrees of freedom of a system, the plots in Fig. 4.2 tell us, that, for a system of given width and temperature, larger β corresponds more degrees of freedom.

Now we move to the next section where we examine the superconducting case. We shall approach the problem in a complete numerical set up.

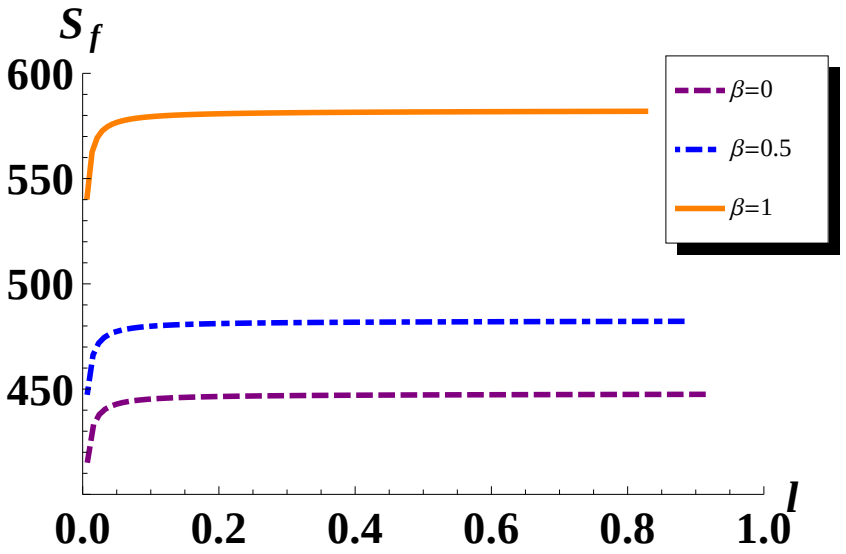

Figure 4.2 Plot of holographic entanglement entropy as a function of the system's strip width l for the AdS-RN black hole with different values of the imbalanced parameter β. Here we have also set $\mu = 1$ and temperature $T_{bh} = 0.13$. Since μ and β are fixed we adjust the horizon radius r_H to keep the temperature constant.

4.5 HEE for the superconducting phase with varying β

We now intend to calculate the HEE when the black hole has developed a scalar hair, in other sense, a superconducting state has been formed in the boundary field theory. It is not possible to compute the hairy black hole metric by staying within analytical

limit. Therefore we approach this problem with the help of numerics.

4.5.1 Field equations and the bulk/boundary expansions

We rewrite the equations of motion (Eq. (4.13) to Eq. (4.17)) by expressing $g(z) = \frac{r_H^2}{z^2} + h(z)$ which is helpful for further computations [74]. In terms of $h(z)$ these look like:

$$\begin{aligned}
&\frac{\phi'^2}{2} + \frac{\phi\phi'}{z} + \frac{\phi^2}{2z^2} + \frac{e^\chi(\psi'^2 + v'^2)}{4(r_H^2 + z^2 h)} - \frac{h'}{z(r_H^2 + z^2 h)} + \frac{m^2 r_H^2 \phi^2}{2z^2(r_H^2 + z^2 h)} \\
+ \;& \frac{1}{z^4} - \frac{r_H^2}{z^4(r_H^2 + z^2 h)} + \frac{e^\chi r_H^2 q^2 \psi^2 \phi^2}{2(r_H^2 + z^2 h)^2} = 0 \qquad (4.35)\\
&\chi' - z\phi^2 - \frac{z^3 e^\chi r_H^2 q^2 \psi^2 \phi^2}{(r_H^2 + z^2 h)^2} - 2z^2\phi\phi' - z^3\phi'^2 = 0 \qquad (4.36)\\
&\frac{\psi''}{r_H^2} + \frac{\psi'\chi'}{2r_H^2} - \frac{2q^2\psi\phi^2}{r_H^2 + z^2 h} = 0 \qquad (4.37)\\
&\frac{v''}{r_H^2} + \frac{v'\chi'}{2r_H^2} = 0 \qquad (4.38)\\
&\phi'' + \left(\frac{2}{z} - \frac{2r_H^2}{z(r_H^2 + z^2 h)} - \frac{\chi'}{2} + \frac{h' z^2}{r_H^2 + z^2 h}\right)\phi' - \frac{r_H^2 m^2 \phi}{2z^2(r_H^2 + z^2 h)} \\
+ \;& \left(-\frac{2r_H^2}{z^2(r_H^2 + z^2 h)} + \frac{q^2 e^\chi r_H^2 \psi^2}{(r_H^2 + z^2 h)^2} - \frac{\chi'}{2z} + \frac{h' z}{r_H^2 + z^2 h}\right)\phi = 0. \qquad (4.39)
\end{aligned}$$

In order to set the stage one needs to translate the problem of finding the hairy black hole into a boundary value problem by using Taylor series expansion of various fields. Near the horizon $z_H = 1$ they are expanded as

$$\begin{aligned}
h_H(z) &= -r_H^2 + h_{H1}(1-z) + h_{H2}(1-z)^2 + \cdots \qquad (4.40)\\
\chi_H(z) &= \chi_{H0} + \chi_{H1}(1-z) + \chi_{H2}(1-z)^2 + \cdots \qquad (4.41)\\
\psi_H(z) &= \psi_{H1}(1-z) + \psi_{H2}(1-z)^2 + \cdots \qquad (4.42)\\
v_H(z) &= v_{H1}(1-z) + v_{H2}(1-z)^2 + \cdots \qquad (4.43)\\
\phi_H(z) &= \phi_{H0} + \phi_{H1}(1-z) + \phi_{H2}(1-z)^2 + \cdots \qquad (4.44)
\end{aligned}$$

Note that in the Taylor expansion of $h_H(z)$, we set the first term as $-r_H^2$ to fulfil the requirement that the metric coefficient $g(z)$ vanishes at the horizon. Also, in order to prevent the gauge fields from acquiring infinite norm at the horizon one needs $\psi_H(z=1) = 0 = v_H(z=1)$. Therefore, upto a second-order expansion, one has twelve unknown coefficients in the Taylor expansions. However not all of them are independent, they are related by five equations (Eq. (4.35) to Eq. (4.39)) and one needs to substitute the field expansions in these equations. This gives a set of algebraic equations which relate various Taylor coefficients in different orders of expansion. Finally one is left with six independent coefficients and all others are expressible in terms of them. We choose these coefficients to be $\phi_{H0}, \chi_{H0}, \psi_{H1}, v_{H1}, q, r_H$. The next step is to find the expressions of dependent Taylor coefficients appearing in the near horizon expansions in terms of these independent parameters. Some of them with relatively simpler expressions are:

$$h_{H1} = -\frac{1}{4}e^{\chi_{H0}}(v_{H1}^2 + \psi_{H1}^2) + r_H^2(1+\phi_{H0}^2) \tag{4.45}$$

$$\chi_{H1} = -\frac{16r_H^2(r_H^2 + e^{\chi_{H0}}q^2\psi_{H1}^2)\phi_{H0}^2}{(e^{\chi_{H0}}(v_{H1}^2+\psi_{H1}^2) - 4r_H^2(3+\phi_{H0}^2))^2} \tag{4.46}$$

$$\phi_{H1} = \phi_{H0} + \frac{4r_H^2\phi_{H0}}{e^{\chi_{H0}}(v_{H1}^2+\psi_{H1}^2) - 4r_H^2(3+\phi_{H0}^2)} \tag{4.47}$$

$$\psi_{H2} = \frac{4r_H^2\psi_{H1}\phi_{H0}^2\left(-e^{\chi_{H0}}q^2v_{H1}^2 + r_H^2\left(1+4q^2\left(3+\phi_{H0}^2\right)\right)\right)}{\left(e^{\chi_{H0}}\left(v_{H1}^2+\psi_{H1}^2\right) - 4r_H^2\left(3+\phi_{H0}^2\right)\right)^2} \tag{4.48}$$

$$v_{H2} = \frac{4r_H^2 v_{H1}\left(e^{\chi_{H0}}q^2\psi_{H1}^2 + r_H^2\right)\phi_{H0}^2}{\left(12r_H^2 - e^{\chi_{H0}}v_{H1}^2 - e^{\chi_{H0}}\psi_{H1}^2 + 4r_H^2\phi_{H0}^2\right)^2}. \tag{4.49}$$

The others are more complicated and are given in the appendix.

Now let us write down the ultraviolet (UV) asymptotic (boundary) behaviour of

all fields near the AdS boundary $z = 0$:

$$h_b(z) = -\frac{\epsilon}{2r_H}z + \cdots \tag{4.50}$$

$$\chi_b(z) = \log(1+a) = 0 \tag{4.51}$$

$$\psi_b(z) = \mu - \frac{\rho\, z}{r_H} + \cdots \tag{4.52}$$

$$v_b(z) = \delta\mu - \frac{\delta\rho\, z}{r_H} + \cdots \tag{4.53}$$

$$\phi_b(z) = \frac{C_1}{r_H} + \frac{C_2}{r_H^2}z + \cdots \tag{4.54}$$

where ϵ is the mass of RN-AdS black hole defined at the spatial asymptote. As usual, both C_1 and C_2 cannot be nonzero at the same time. Here our aim is to solve the boundary value problem with $C_1 = 0$ but $C_2 \neq 0$. The reason behind this is that C_2 has conformal mass dimension 2 which corresponds to $\Delta = 2$ of the Fermionic operator representing the condensate.

4.5.2 Numerical scheme for finding the hairy black hole

Here we look for the solution of the above set of equations in order to compute the hairy black hole metric. Our focus thus is on getting the solution for $h(z)$. We use the shooting method for this purpose. Here the basic idea for solving the boundary value problem is to first express various boundary parameters in terms of near horizon

fields and their derivatives. For that one inverts the above set of equations to write

$$\mu = \psi_b(z) - z\psi_b'(z), \tag{4.55}$$

$$\rho = -r_H\psi_b'(z), \tag{4.56}$$

$$C_1 = \phi_b(z)r_H - \phi_b'(z)r_H z, \tag{4.57}$$

$$C_2 = \phi_b'(z)r_H^2, \tag{4.58}$$

$$a = e^{-\chi_b(z)} - 1, \tag{4.59}$$

$$\epsilon = -2r_H h_b'(z), \tag{4.60}$$

$$\delta\rho = -r_H v_b'(z), \tag{4.61}$$

$$\delta\mu = v_b(z) - zv_b'(z). \tag{4.62}$$

The temperature of this superconducting state is also given in terms of near horizon expressions, given by [74]

$$T_{sc} = \frac{r_H}{16\pi}\left((12 + 4\phi_{H0}^2)e^{-\frac{\chi_{H0}}{2}} - \frac{1}{r_H^2}e^{\frac{\chi_{H0}}{2}}(\psi_{H1}^2 + v_{H1}^2)\right). \tag{4.63}$$

The critical temperature corresponds to the smallest possible value of ϕ_{H0} such that the hair is just developed.

In the numerical scheme we set a very small value for ϕ_{H0} and all other parameters are fixed by hand and they are provided as the input *seed* to solve the set of coupled differential equations. Then in the following step we make a very small increment for the seed of ϕ_{H0} and that will determine other near horizon parameters which, together, will set the input values for the second step. Moreover, at every step, one finds the values of various UV parameters (Eq. (4.55) to Eq. (4.62)) as a part of the output. In this way one generates a set of data of solutions by implementing this iteration for a number of times. For each iteration one has numerical values for–(i) near-horizon parameters and (ii) boundary parameters as a function of that. It is then trivial to reproduce $h(z)$ as well as the metric $g(z)$. Furthermore at each step

we get a temperature given by Eq. (4.63). As we mentioned earlier that our aim is to find the hairy black hole solution so that we can use that for the further computation of the HEE.

In Fig. 4.3 we plot the family of hairy black hole metrics $g(z)$ for two cases with $\beta = 0.01$ and $\beta = 0.02$. For a fixed imbalanced parameter, different plots correspond to distinct temperatures which in our case are very close to each other. Subsequently we shall choose one of these metrics with a particular temperature and compute the HEE to compare with the black hole phase.

Before going further some words about our code are in order. As usual, while solving the boundary value problem the issues with divergences are tackled by propagating the near horizon solutions from $\epsilon_H = 0.00001$ away from the horizon ($z = 1$) to $\epsilon_b = 0.000001$ near the boundary ($z = 0$). As the boundary conditions we have set $C_1 = 0, a = 0, \mu = 1$ and $\delta\mu = 0.01$ for one case while $\delta\mu = 0.02$ for the other. In all cases we have set $q = 2$.

Now we move to the final part where we calculate the HEE for the superconducting phase and compare with the black hole phase.

4.5.3 HEE for the superconducting phase and comparison with the black hole phase

Having found the metric functions $g(z)$ and corresponding temperatures we are free to choose one entry of this set and use Eq. (4.31) and Eq. (4.34) with varying z_0 to obtain the list required for plotting S_f as a function of l. In order to compare with the AdS-RN black hole phase we fix the black hole temperature T_{bh} (Eq. (4.23)) to be equal to the preassigned temperature for the superconducting phase (given by Eq. (4.63)) by suitably adjusting its horizon radius (since μ and $\delta\mu$ are already fixed).

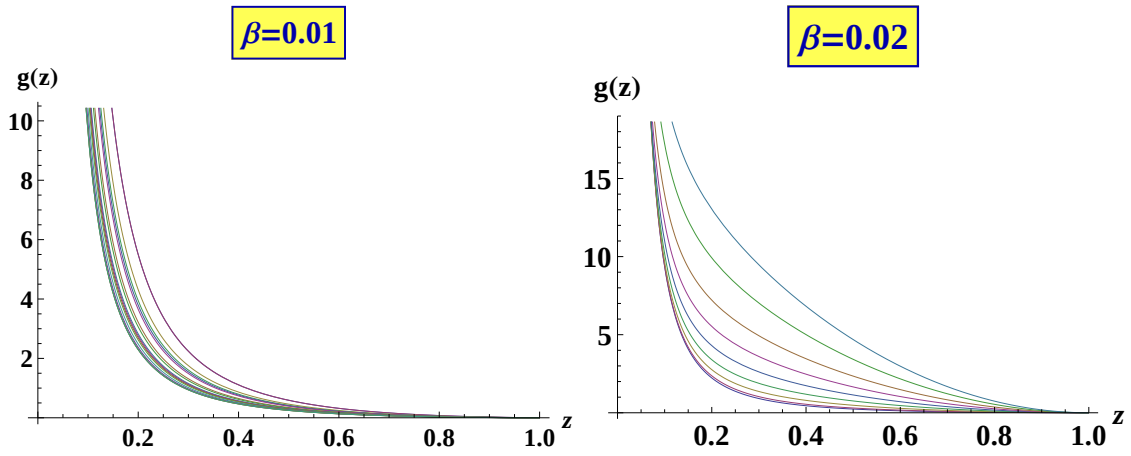

Figure 4.3 Plot of the hairy black hole metric function with respect to the radial coordinate z as obtained from numerical computations. As expected $g(z)$ vanishes at the horizon and diverges at asymptotic infinity. Different curves in this plot correspond to different characteristic temperature.

With this new horizon radius then we use the black hole metric to calculate the list for the required plot.

In Fig. 4.4 we compare the relative values of the HEE between the black hole and superconducting states for fixed (i) chemical potential $\mu = 1$, (ii) imbalance parameter $\beta = 0.01,\ 0.02$ respectively and (iii) identical values of temperatures $T_{bh} = T_{sc}$ for each β. From both of these plots we note that the superconducting state has a lower HEE than the normal (RN-AdS) state. This, as explained by Albash et al [124], represents the fact that the degrees of freedom have condensed from the RN-AdS case to the superconducting state and may serve the purpose of signaling the preferable state.

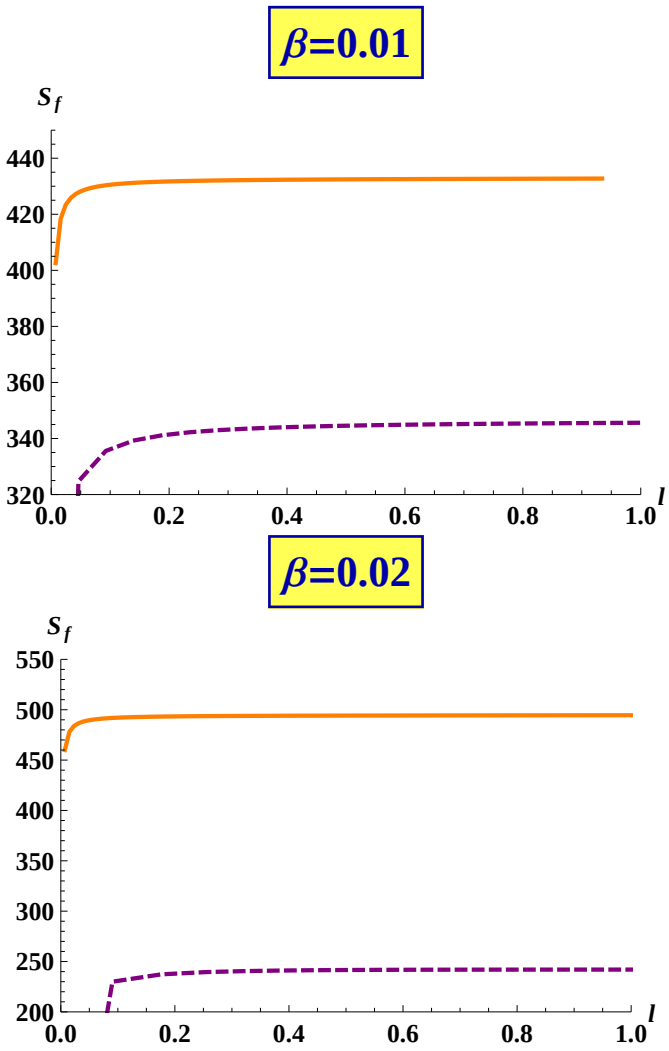

Figure 4.4 Plot of holographic entanglement entropy of AdS-RN black hole (solid lines) and imbalanced superconductors (dashed lines) at $T_{bh} = T_{sc} = 0.13$ for $\beta = 0.01$ and $\beta = 0.02$. The results remain similar if we choose any other temperature and $g(z)$ from Fig. 4.3. For other details refer to text.

4.5.4 Variation of HEE with β for the holographic superconductor

Finally we are in a position to compare the change in HEE for the superconducting phase for different imbalances while all other parameters are kept fixed. For this we do

not need to perform anymore computations, rather, we compare the superconducting phase plots from Fig. 4.4. This is depicted in Fig. 4.5 which shows that with the increase in chemical imbalance HEE decreases. Notably this behaviour is exactly opposite to the RN-AdS phase as shown in Fig. 4.2.

In order to understand this difference physically one should consider the fact that thermodynamics of AdS black holes may differ substantially from a physical system like superconductors. For example if we, keeping the horizon radius constant, increase β then temperature of the RN-AdS black hole as given by Eq. (4.23) becomes smaller. On the other hand one can check that HEE increases with the increase β for constant horizon radius. Since HEE in certain cases resembles with the black hole entropy [123] one can roughly interpret this behaviour in terms of the negative specific heat of black holes. It is known that in certain cases AdS black holes do have negative specific heat [134]. On the other hand one expects a superconducting system to have a positive heat capacity and therefore the difference with the black hole phase is natural.

On the other hand this behaviour might challenge the HEE to correctly identify the preferable state. The fact that HEE for black hole phase increases while it decreases for the superconducting state implies that for larger chemical potential imbalance superconducting state will be more probable. Of course this goes against the fact that with arbitrarily large imbalance one cannot achieve superconductivity. Therefore one should be careful in interpreting physics of holographic superconductors only by looking at the HEE.

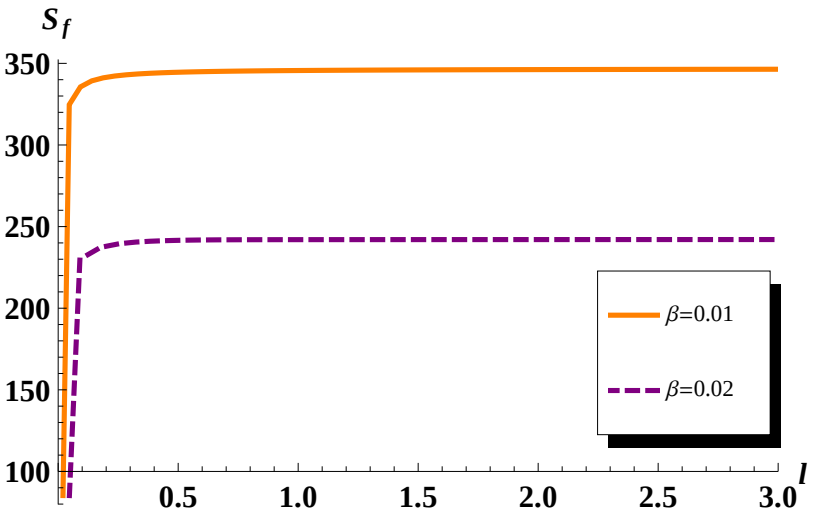

Figure 4.5 Plot of holographic entanglement entropy of the superconducting phase for two different chemical imbalances. In these plots $\mu = 1$ and $T_{sc} = 0.13$ for both cases. The results remain similar if we choose any other temperature and $g(z)$ from Fig. 4.3. Details are given in text.

4.6 Summary and Discussion

In this work presented in this chapter, we computed Holographic entanglement entropy (HEE) starting from a fully back-reacted gravitational theory which describes imbalanced superconductivity below the critical temperature and doubly-charged RN-AdS black hole at temperature higher than the critical temperature. We chose the strip geometry for the entangled surface and compute the HEE as a function of strip size. The hairy black hole metric was found by using the numerical shooting method. Results showed that HEE for the superconducting state is lower than the black hole/normal phase for the values of the imbalance parameter (β) considered in this work. It was also shown that the effect of the imbalance is exactly opposite

for black hole and superconducting phases. For the AdS-RN black hole phase HEE increases with the increase in the imbalance in two chemical potentials. Whereas for holographic superconductor HEE decreases. The fact that HEE for imbalanced holographic superconductor (also for other cases reported earlier [124]- [127]) is less than the black hole might insist one to consider this as a good physical parameter to identify the preferable state below T_c.

The present study also raises a question whether or not HEE *alone* can always correctly identify the preferable state for physical systems like imbalanced mixtures. The fact that HEE increases for the black hole phase and decreases for superconducting phase with respect to increasing imbalance imply that superconducting state will be more and more preferable as imbalance increases. But, as known from physical considerations, this is not the case with imbalanced systems. So clearly HEE fails to serve this purpose in this context. Usually for a condensed matter system one uses free energy in order to say anything about the preferable state. With the concern we mentioned it is unlikely that HEE alone could serve the purpose of free energy for holographic superconductors.

4.7 Appendix

For the sake of completeness and future reference, in this appendix we provide the expressions of h_{H2}, χ_{H2} and ϕ_{H2} in terms of the independent parameters $\phi_{H0}, \chi_{H0}, \psi_{H1}, v_{H1}, q, r_H$.

$$
\begin{aligned}
h_{H2} = \frac{1}{4q^2 r_H^2 \phi_{H0}^2 \psi_{H1}^2}(&-7q^2\phi_{H0}^2\psi_{H1}^2 r_H^4 + 10q^2\phi_{H0}\phi_{H1}\psi_{H1}^2 r_H^4 - 4q^2\phi_{H0}^2\psi_{H1}\psi_{H2} r_H^4 \\
&+ 3h_{H1}q^2\phi_{H0}^2\psi_{H1}^2 r_H^2 + 5h_{H1}q^2\phi_{H0}\phi_{H1}\psi_{H1}^2 r_H^2 - 2h_{H1}q^2\phi_{H0}^2\psi_{H1}\psi_{H2} r_H^2 \\
&\pm (-7q^4\phi_{H0}^4\psi_{H1}^4 r_H^8 + 36q^4\phi_{H0}^2\phi_{H1}^2\psi_{H1}^4 r_H^8 - 236q^4\phi_{H0}^3\phi_{H1}\psi_{H1}^4 r_H^8 \\
&+ 16q^4\phi_{H0}^4\chi_{H1}\psi_{H1}^4 r_H^8 - 16q^4\phi_{H0}^3\phi_{H1}\chi_{H1}\psi_{H1}^4 r_H^8 + 144q^4\phi_{H0}^4\psi_{H1}^2\psi_{H2}^2 r_H^8 \\
&- 128q^2\phi_{H0}^2\chi_{H1}\psi_{H1}^2\psi_{H2}^2 r_H^8 + 88q^4\phi_{H0}^4\psi_{H1}^3\psi_{H2} r_H^8 + 48q^4\phi_{H0}^3\phi_{H1}\psi_{H1}^3\psi_{H2} r_H^8 \\
&+ 8e^{\chi_{H0}}q^6\phi_{H0}^4\psi_{H1}^6 r_H^6 - 98h_{H1}q^4\phi_{H0}^4\psi_{H1}^4 r_H^6 + 36h_{H1}q^4\phi_{H0}^2\phi_{H1}^2\psi_{H1}^4 r_H^6 \\
&- 234h_{H1}q^4\phi_{H0}^3\phi_{H1}\psi_{H1}^4 r_H^6 + 16h_{H1}q^4\phi_{H0}^4\chi_{H1}\psi_{H1}^4 r_H^6 - 16h_{H1}q^4\phi_{H0}^3\phi_{H1}\chi_{H1}\psi_{H1}^4 r_H^6 \\
&+ 144h_{H1}q^4\phi_{H0}^4\psi_{H1}^2\psi_{H2}^2 r_H^6 - 192h_{H1}q^2\phi_{H0}^2\chi_{H1}\psi_{H1}^2\psi_{H2}^2 r_H^6 + 84h_{H1}q^4\phi_{H0}^4\psi_{H1}^3\psi_{H2} r_H^6 \\
&+ 48h_{H1}q^4\phi_{H0}^3\phi_{H1}\psi_{H1}^3\psi_{H2} r_H^6 - 47h_{H1}^2q^4\phi_{H0}^4\psi_{H1}^4 r_H^4 + 9h_{H1}^2q^4\phi_{H0}^2\phi_{H1}^2\psi_{H1}^4 r_H^4 \\
&- 58h_{H1}^2q^4\phi_{H0}^3\phi_{H1}\psi_{H1}^4 r_H^4 + 4h_{H1}^2q^4\phi_{H0}^4\chi_{H1}\psi_{H1}^4 r_H^4 - 4h_{H1}^2q^4\phi_{H0}^3\phi_{H1}\chi_{H1}\psi_{H1}^4 r_H^4 \\
&+ 36h_{H1}^2q^4\phi_{H0}^4\psi_{H1}^2\psi_{H2}^2 r_H^4 - 96h_{H1}^2q^2\phi_{H0}^2\chi_{H1}\psi_{H1}^2\psi_{H2}^2 r_H^4 + 20h_{H1}^2q^4\phi_{H0}^4\psi_{H1}^3\psi_{H2} r_H^4 \\
&+ 12h_{H1}^2q^4\phi_{H0}^3\phi_{H1}\psi_{H1}^3\psi_{H2} r_H^4 - 16h_{H1}^3q^2\phi_{H0}^2\chi_{H1}\psi_{H1}^2\psi_{H2}^2 r_H^2)^{1/2})
\end{aligned}
\tag{4.64}
$$

$$\chi_{H2} = \frac{1}{\psi_{H1}}\Bigg(\frac{2q^2\phi_{H0}^2\psi_{H2}r_H^4}{(2r_H^2+h_{H1})^2} - \frac{5q^2\phi_{H0}\phi_{H1}\psi_{H1}r_H^4}{(2r_H^2+h_{H1})^2} - \frac{5q^2\phi_{H0}^2\psi_{H1}r_H^4}{2(2r_H^2+h_{H1})^2}$$
$$+ \frac{4q^2\phi_{H0}^2\psi_{H1}r_H^2}{2r_H^2+h_{H1}} + \frac{4q^2\phi_{H0}\phi_{H1}\psi_{H1}r_H^2}{2r_H^2+h_{H1}} + \frac{2q^2\phi_{H0}^2\psi_{H2}r_H^2}{2r_H^2+h_{H1}}$$
$$+ \frac{h_{H1}q^2\phi_{H0}^2\psi_{H2}r_H^2}{(2r_H^2+h_{H1})^2} - \frac{3h_{H1}q^2\phi_{H0}^2\psi_{H1}r_H^2}{2(2r_H^2+h_{H1})^2} - \frac{5h_{H1}q^2\phi_{H0}\phi_{H1}\psi_{H1}r_H^2}{2(2r_H^2+h_{H1})^2}$$
$$- \chi_{H1}\psi_{H2} \pm \frac{1}{2(2r_H^2+h_{H1})^2\psi_{H1}}\Bigg((-7q^4\phi_{H0}^4\psi_{H1}^4r_H^8 + 36q^4\phi_{H0}^2\phi_{H1}^2\psi_{H1}^4r_H^8$$
$$- 236q^4\phi_{H0}^3\phi_{H1}\psi_{H1}^4r_H^8 + 16q^4\phi_{H0}^4\chi_{H1}\psi_{H1}^4r_H^8 - 16q^4\phi_{H0}^3\phi_{H1}\chi_{H1}\psi_{H1}^4r_H^8$$
$$+ 144q^4\phi_{H0}^4\psi_{H1}^2\psi_{H2}^2r_H^8 - 128q^2\phi_{H0}^2\chi_{H1}\psi_{H1}^2\psi_{H2}^2r_H^8 + 88q^4\phi_{H0}^4\psi_{H1}^3\psi_{H2}r_H^8$$
$$+ 48q^4\phi_{H0}^3\phi_{H1}\psi_{H1}^3\psi_{H2}r_H^8 + 8e^{\chi_{H0}}q^6\phi_{H0}^4\psi_{H1}^6r_H^6 - 98h_{H1}q^4\phi_{H0}^4\psi_{H1}^4r_H^6$$
$$+ 36h_{H1}q^4\phi_{H0}^2\phi_{H1}^2\psi_{H1}^4r_H^6 - 234h_{H1}q^4\phi_{H0}^3\phi_{H1}\psi_{H1}^4r_H^6 + 16h_{H1}q^4\phi_{H0}^4\chi_{H1}\psi_{H1}^4r_H^6$$
$$- 16h_{H1}q^4\phi_{H0}^3\phi_{H1}\chi_{H1}\psi_{H1}^4r_H^6 + 144h_{H1}q^4\phi_{H0}^4\psi_{H1}^2\psi_{H2}^2r_H^6 - 192h_{H1}q^2\phi_{H0}^2\chi_{H1}\psi_{H1}^2\psi_{H2}^2r_H^6$$
$$+ 84h_{H1}q^4\phi_{H0}^4\psi_{H1}^3\psi_{H2}r_H^6 + 48h_{H1}q^4\phi_{H0}^3\phi_{H1}\psi_{H1}^3\psi_{H2}r_H^6 - 47h_{H1}^2q^4\phi_{H0}^4\psi_{H1}^4r_H^4$$
$$+ 9h_{H1}^2q^4\phi_{H0}^2\phi_{H1}^2\psi_{H1}^4r_H^4 - 58h_{H1}^2q^4\phi_{H0}^3\phi_{H1}\psi_{H1}^4r_H^4 + 4h_{H1}^2q^4\phi_{H0}^4\chi_{H1}\psi_{H1}^4r_H^4$$
$$- 4h_{H1}^2q^4\phi_{H0}^3\phi_{H1}\chi_{H1}\psi_{H1}^4r_H^4 + 36h_{H1}^2q^4\phi_{H0}^4\psi_{H1}^2\psi_{H2}^2r_H^4 - 96h_{H1}^2q^2\phi_{H0}^2\chi_{H1}\psi_{H1}^2\psi_{H2}^2r_H^4$$
$$+ 20h_{H1}^2q^4\phi_{H0}^4\psi_{H1}^3\psi_{H2}r_H^4 + 12h_{H1}^2q^4\phi_{H0}^3\phi_{H1}\psi_{H1}^3\psi_{H2}r_H^4 - 16h_{H1}^3q^2\phi_{H0}^2\chi_{H1}\psi_{H1}^2\psi_{H2}^2r_H^2)^{1/2}\Bigg)\Bigg) \tag{4.65}$$

$$\phi_{H2} = \frac{1}{8}\Bigg(\frac{5\phi_{H0} r_H^4}{2(2r_H^2 + h_{H1})^2} + \frac{5\phi_{H1} r_H^4}{(2r_H^2 + h_{H1})^2} - \frac{2\phi_{H0}\psi_{H2} r_H^4}{(2r_H^2 + h_{H1})^2 \psi_{H1}}$$
$$+ \frac{3h_{H1}\phi_{H0} r_H^2}{2(2r_H^2 + h_{H1})^2} + \frac{\phi_{H1} r_H^2}{2(2r_H^2 + h_{H1})} + \frac{5h_{H1}\phi_{H1} r_H^2}{2(2r_H^2 + h_{H1})^2} + \frac{2\phi_{H1}\psi_{H2} r_H^2}{(2r_H^2 + h_{H1})\psi_{H1}}$$
$$- \frac{11\phi_{H0} r_H^2}{2(2r_H^2 + h_{H1})} - \frac{2e^{\chi_{H0}} q^2 \phi_{H0}\psi_{H1}^2 r_H^2}{(2r_H^2 + h_{H1})^2} - \frac{5\phi_{H1}^2 r_H^2}{(2r_H^2 + h_{H1})\phi_{H0}}$$
$$- \frac{2\phi_{H0}\psi_{H2} r_H^2}{(2r_H^2 + h_{H1})\psi_{H1}} - \frac{h_{H1}\phi_{H0}\psi_{H2} r_H^2}{(2r_H^2 + h_{H1})^2 \psi_{H1}} + \frac{3h_{H1}\phi_{H0}}{2(2r_H^2 + h_{H1})}$$
$$+ 2\phi_{H0} + \frac{h_{H1}\phi_{H1}}{2r_H^2 + h_{H1}} + 6\phi_{H1} - \phi_{H0}\chi_{H1} + \phi_{H1}\chi_{H1} + \frac{h_{H1}\phi_{H1}\psi_{H2}}{(2r_H^2 + h_{H1})\psi_{H1}}$$
$$\pm \frac{1}{2q^2 r_H^2 (2r_H^2 + h_{H1})\phi_{H0}\psi_{H1}^2} \Bigg((-7q^4\phi_{H0}^4\psi_{H1}^4 r_H^8 + 36q^4\phi_{H0}^2\phi_{H1}^2\psi_{H1}^4 r_H^8$$
$$- 236q^4\phi_{H0}^3\phi_{H1}\psi_{H1}^4 r_H^8 + 16q^4\phi_{H0}^4\chi_{H1}\psi_{H1}^4 r_H^8 - 16q^4\phi_{H0}^3\phi_{H1}\chi_{H1}\psi_{H1}^4 r_H^8$$
$$+ 144q^4\phi_{H0}^4\psi_{H1}^2\psi_{H2}^2 r_H^8 - 128q^2\phi_{H0}^2\chi_{H1}\psi_{H1}^2\psi_{H2}^2 r_H^8 + 88q^4\phi_{H0}^4\psi_{H1}^3\psi_{H2} r_H^8$$
$$+ 48q^4\phi_{H0}^3\phi_{H1}\psi_{H1}^3\psi_{H2} r_H^8 + 8e^{\chi_{H0}} q^6\phi_{H0}^4\psi_{H1}^6 r_H^6 - 98h_{H1}q^4\phi_{H0}^4\psi_{H1}^4 r_H^6$$
$$+ 36h_{H1}q^4\phi_{H0}^2\phi_{H1}^2\psi_{H1}^4 r_H^6 - 234h_{H1}q^4\phi_{H0}^3\phi_{H1}\psi_{H1}^4 r_H^6 + 16h_{H1}q^4\phi_{H0}^4\chi_{H1}\psi_{H1}^4 r_H^6$$
$$- 16h_{H1}q^4\phi_{H0}^3\phi_{H1}\chi_{H1}\psi_{H1}^4 r_H^6 + 144h_{H1}q^4\phi_{H0}^4\psi_{H1}^2\psi_{H2}^2 r_H^6 - 192h_{H1}q^2\phi_{H0}^2\chi_{H1}\psi_{H1}^2\psi_{H2}^2 r_H^6$$
$$+ 84h_{H1}q^4\phi_{H0}^4\psi_{H1}^3\psi_{H2} r_H^6 + 48h_{H1}q^4\phi_{H0}^3\phi_{H1}\psi_{H1}^3\psi_{H2} r_H^6 - 47h_{H1}^2 q^4\phi_{H0}^4\psi_{H1}^4 r_H^4$$
$$+ 9h_{H1}^2 q^4\phi_{H0}^2\phi_{H1}^2\psi_{H1}^4 r_H^4 - 58h_{H1}^2 q^4\phi_{H0}^3\phi_{H1}\psi_{H1}^4 r_H^4 + 4h_{H1}^2 q^4\phi_{H0}^4\chi H1\psi_{H1}^4 r_H^4$$
$$- 4h_{H1}^2 q^4\phi_{H0}^3\phi_{H1}\chi_{H1}\psi_{H1}^4 r_H^4 + 36h_{H1}^2 q^4\phi_{H0}^4\psi_{H1}^2\psi_{H2}^2 r_H^4 - 96h_{H1}^2 q^2\phi_{H0}^2\chi H1\psi_{H1}^2\psi_{H2}^2 r_H^4$$
$$+ 20h_{H1}^2 q^4\phi_{H0}^4\psi_{H1}^3\psi_{H2} r_H^4 + 12h_{H1}^2 q^4\phi_{H0}^3\phi_{H1}\psi_{H1}^3\psi_{H2} r_H^4 - 16h_{H1}^3 q^2\phi_{H0}^2\chi H1\psi_{H1}^2\psi_{H2}^2 r_H^2)^{1/2} \Bigg)$$
$$- \frac{5h_{H1}\phi_{H1}^2}{2(2r_H^2 + h_{H1})\phi_{H0}} - \frac{h_{H1}\phi_{H0}\psi_{H2}}{(2r_H^2 + h_{H1})\psi_{H1}} \pm \frac{1}{2q^2(2r_H^2 + h_{H1})^2\phi_{H0}\psi_{H1}^2}$$
$$\Bigg(\Bigg(- 7q^4\phi_{H0}^4\psi_{H1}^4 r_H^8 + 36q^4\phi_{H0}^2\phi_{H1}^2\psi_{H1}^4 r_H^8 - 236q^4\phi_{H0}^3\phi_{H1}\psi_{H1}^4 r_H^8$$
$$+ 16q^4\phi_{H0}^4\chi H1\psi_{H1}^4 r_H^8 - 16q^4\phi_{H0}^3\phi_{H1}\chi H1\psi_{H1}^4 r_H^8 + 144q^4\phi_{H0}^4\psi_{H1}^2\psi_{H2}^2 r_H^8$$
$$- 128q^2\phi_{H0}^2\chi H1\psi_{H1}^2\psi_{H2}^2 r_H^8 + 88q^4\phi_{H0}^4\psi_{H1}^3\psi_{H2} r_H^8 + 48q^4\phi_{H0}^3\phi_{H1}\psi_{H1}^3\psi_{H2} r_H^8$$
$$+ 8e^{\chi H0} q^6\phi_{H0}^4\psi_{H1}^6 r_H^6 - 98h_{H1}q^4\phi_{H0}^4\psi_{H1}^4 r_H^6 + 36h_{H1}q^4\phi_{H0}^2\phi_{H1}^2\psi_{H1}^4 r_H^6$$
$$- 234h_{H1}q^4\phi_{H0}^3\phi_{H1}\psi_{H1}^4 r_H^6 + 16h_{H1}q^4\phi_{H0}^4\chi H1\psi_{H1}^4 r_H^6 - 16h_{H1}q^4\phi_{H0}^3\phi_{H1}\chi H1\psi_{H1}^4 r_H^6$$
$$+ 144h_{H1}q^4\phi_{H0}^4\psi_{H1}^2\psi_{H2}^2 r_H^6 - 192h_{H1}q^2\phi_{H0}^2\chi H1\psi_{H1}^2\psi_{H2}^2 r_H^6 + 84h_{H1}q^4\phi_{H0}^4\psi_{H1}^3\psi_{H2} r_H^6$$

$$+ 48h_{H1}q^4\phi_{H0}^3\phi_{H1}\psi_{H1}^3\psi_{H2}r_H^6 - 47h_{H1}^2q^4\phi_{H0}^4\psi_{H1}^4r_H^4 + 9h_{H1}^2q^4\phi_{H0}^2\phi_{H1}^2\psi_{H1}^4r_H^4$$

$$- 58h_{H1}^2q^4\phi_{H0}^3\phi_{H1}\psi_{H1}^4r_H^4 + 4h_{H1}^2q^4\phi_{H0}^4\chi H1\psi_{H1}^4r_H^4 - 4h_{H1}^2q^4\phi_{H0}^3\phi_{H1}\chi H1\psi_{H1}^4r_H^4$$

$$+ 36h_{H1}^2q^4\phi_{H0}^4\psi_{H1}^2\psi_{H2}^2r_H^4 - 96h_{H1}^2q^2\phi_{H0}^2\chi H1\psi_{H1}^2\psi_{H2}^2r_H^4 + 20h_{H1}^2q^4\phi_{H0}^4\psi_{H1}^3\psi_{H2}r_H^4$$

$$+ 12h_{H1}^2q^4\phi_{H0}^3\phi_{H1}\psi_{H1}^3\psi_{H2}r_H^4 - 16h_{H1}^3q^2\phi_{H0}^2\chi H1\psi_{H1}^2\psi_{H2}^2r_H^2\Big)^{1/2}\Big) - \frac{5h_{H1}\phi_{H1}^2}{2(2r_H^2 + h_{H1})\phi_{H0}}$$

$$- \frac{h_{H1}\phi_{H0}\psi_{H2}}{(2r_H^2 + h_{H1})\psi_{H1}} \pm \frac{1}{2q^2r_H^2(2r_H^2 + h_{H1})\phi_{H0}^2\psi_{H1}^2}\phi_{H1}$$

$$\Big(- 7q^4\phi_{H0}^4\psi_{H1}^4r_H^8 + 36q^4\phi_{H0}^2\phi_{H1}^2\psi_{H1}^4r_H^8 - 236q^4\phi_{H0}^3\phi_{H1}\psi_{H1}^4r_H^8 + 16q^4\phi_{H0}^4\chi H1\psi_{H1}^4r_H^8$$

$$- 16q^4\phi_{H0}^3\phi_{H1}\chi H1\psi_{H1}^4r_H^8 + 144q^4\phi_{H0}^4\psi_{H1}^2\psi_{H2}^2r_H^8 - 128q^2\phi_{H0}^2\chi H1\psi_{H1}^2\psi_{H2}^2r_H^8$$

$$+ 88q^4\phi_{H0}^4\psi_{H1}^3\psi_{H2}r_H^8 + 48q^4\phi_{H0}^3\phi_{H1}\psi_{H1}^3\psi_{H2}r_H^8 + 8e^{\chi H0}q^6\phi_{H0}^4\psi_{H1}^6r_H^6$$

$$- 98h_{H1}q^4\phi_{H0}^4\psi_{H1}^4r_H^6 + 36h_{H1}q^4\phi_{H0}^2\phi_{H1}^2\psi_{H1}^4r_H^6 - 234h_{H1}q^4\phi_{H0}^3\phi_{H1}\psi_{H1}^4r_H^6$$

$$+ 16h_{H1}q^4\phi_{H0}^4\chi H1\psi_{H1}^4r_H^6 - 16h_{H1}q^4\phi_{H0}^3\phi_{H1}\chi H1\psi_{H1}^4r_H^6 + 144h_{H1}q^4\phi_{H0}^4\psi_{H1}^2\psi_{H2}^2r_H^6$$

$$- 192h_{H1}q^2\phi_{H0}^2\chi H1\psi_{H1}^2\psi_{H2}^2r_H^6 + 84h_{H1}q^4\phi_{H0}^4\psi_{H1}^3\psi_{H2}r_H^6 + 48h_{H1}q^4\phi_{H0}^3\phi_{H1}\psi_{H1}^3\psi_{H2}r_H^6$$

$$- 47h_{H1}^2q^4\phi_{H0}^4\psi_{H1}^4r_H^4 + 9h_{H1}^2q^4\phi_{H0}^2\phi_{H1}^2\psi_{H1}^4r_H^4 - 58h_{H1}^2q^4\phi_{H0}^3\phi_{H1}\psi_{H1}^4r_H^4$$

$$+ 4h_{H1}^2q^4\phi_{H0}^4\chi H1\psi_{H1}^4r_H^4 - 4h_{H1}^2q^4\phi_{H0}^3\phi_{H1}\chi H1\psi_{H1}^4r_H^4 + 36h_{H1}^2q^4\phi_{H0}^4\psi_{H1}^2\psi_{H2}^2r_H^4$$

$$- 96h_{H1}^2q^2\phi_{H0}^2\chi H1\psi_{H1}^2\psi_{H2}^2r_H^4 + 20h_{H1}^2q^4\phi_{H0}^4\psi_{H1}^3\psi_{H2}r_H^4 + 12h_{H1}^2q^4\phi_{H0}^3\phi_{H1}\psi_{H1}^3\psi_{H2}r_H^4$$

$$- 16h_{H1}^3q^2\phi_{H0}^2\chi H1\psi_{H1}^2\psi_{H2}^2r_H^2\Big)^{1/2}\Big)\Big) \tag{4.66}$$

Chapter 5

Epilogue

In this last chapter we will summarize this thesis by focussing on the main results and by discussing about the future prospects of our work.

Our aim in this thesis is to study different aspects of unusual imbalanced superconductivity. To that end, in chapter 1 after presenting, in some short sections, the basic properties of superconductivity, we have detailed a general overview of imbalanced superconductors in terms of both theoretical and experimental findings. We have also incorporated a short motivation for studying holographic imbalanced superconductors in this thesis. In chapter 2, we studied a two-component, spin-polarized Fermi gas using a novel mean-field, phenomenological Ginzburg-Landau free energy functional with two competing order parameters. Our findings capture the basic features of the experiment done by Shin et al [17]. This free energy is also shown to support a tricritical point which is different from the conventional one. The specific heat is different from the standard theory. In continuation to this chapter, in chapter 3, we derive the phase diagram of FFLO superconducting state using Ginzburg-Landau free energy. After outlining its derivation from the microscopic Hamiltonian of the system in detail, we find that it has a very clear Lifshitz tricritical point. We find the specific

heat jumps abruptly near the first-order line in the emergent phase diagram which is very similar to the recent experimental observation in layered organic superconductor by Lortz et al [65]. We also show that the region of the phase diagram where the specific heat jumps can be probed by doing a dynamical analysis of the free energy.

After studying imbalanced superconductivity in the weak coupling limit in the previous two chapters, in chapter 4 we study the behaviour of holographic entanglement entropy (HEE) for imbalanced holographic superconductors which is a strongly-coupled superconductor by construction. To calculate the HEE, we employ numerical shooting method and consider the robust case of fully back-reacted gravity system. The hairy black hole solution, calculated using numerical method, is then used to compute the HEE for the superconducting case. The cases we study show that in presence of a mismatch between two chemical potentials, below the critical temperature, superconducting phase has a lower HEE in comparison to the AdS-Reissner-Nordström black hole phase. It is observed that the effect of chemical imbalance are different in the contexts of black hole and superconducting phases. For black hole, HEE increases with increasing imbalance parameter while it behaves oppositely for the superconducting phase. The implications of these results are discussed.

Let us conclude this thesis by outlining some interesting prospects of future research which our thesis opens up:

- Inclusion of higher order gradient terms in the free energy proposed in chapter 2 may lead to a new phase diagram. Logically it seems that it will be similar to the phase diagram presented in chapter 3, but it needs to be confirmed as it may reveal a connection between Sarma and FFLO states.

- A time-dependent Ginzburg-Landau analysis of the aforesaid free energy will be another worthwhile problem. The connection of this study with the dynamical

studies performed in microscopic Hubbard-like models may provide some new insights.

- To extend the dynamical study of the GL free energy in chapter 3 beyond Hartree approximation and see what it results in.

- To study covariant holographic entanglement entropy of imbalanced holographic superconductor.

The study of unusual imbalanced superconductivity is an interesting and interdisciplinary problem and there are many unknown avenues left for exploration. We hope that the studies presented in the present thesis provide a better understanding of the present scenario and will lead to fruitful future research.

The Road goes ever on and on
Down from the door where it began.
Now far ahead the Road has gone,
And I must follow, if I can,
Pursuing it with eager feet,
Until it joins some larger way,
Where many paths and errands meet.
And whither then? I cannot say.

The Fellowship of the Ring
J. R. R. Tolkien (1892–1973)

Bibliography

[1] H. K. Onnes., Leiden Comm. 120b, 122b, 124c (1911).

[2] *Nobel Lectures, Physics 1901-1921* (Elsevier Publishing Company, Amsterdam, 1967).

[3] J. Hirsch, "The Lorentz force and superconductivity," Physics Letters A **315,** 474 – 479 (2003).

[4] L. N. Cooper, "Bound Electron Pairs in a Degenerate Fermi Gas," Phys. Rev. **104,** 1189–1190 (1956).

[5] J. Bardeen, L. N. Cooper, and J. R. Schrieffer, "Microscopic Theory of Superconductivity," Phys. Rev. **106,** 162–164 (1957).

[6] J. Bardeen, L. N. Cooper, and J. R. Schrieffer, "Theory of Superconductivity," Phys. Rev. **108,** 1175–1204 (1957).

[7] L. D. Landau and V. L. Ginzburg, "On the theory of superconductivity," Journal of Experimental and Theoretical Physics (USSR) **20,** 1064 (1950).

[8] L. P. Gorkov, "Microscopic derivation of the Ginzburg-Landau equations in the theory of superconductivity," Sov. Phys. JETP **9,** 1364–1367 (1959).

[9] A. M. Clogston, "Upper Limit for the Critical Field in Hard Superconductors," Phys. Rev. Lett. **9,** 266–267 (1962).

[10] B. S. Chandrasekhar, "A NOTE ON THE MAXIMUM CRITICAL FIELD OF HIGH-FIELD SUPERCONDUCTORS," Applied Physics Letters **1,** 7–8 (1962).

[11] Y. Matsuda and H. Shimahara, "Fulde–Ferrell–Larkin–Ovchinnikov State in Heavy Fermion Superconductors," Journal of the Physical Society of Japan **76,** 051005 (2007).

[12] G. Sarma, "On the influence of a uniform exchange field acting on the spins of the conduction electrons in a superconductor," Journal of Physics and Chemistry of Solids **24,** 1029 – 1032 (1963).

[13] W. V. Liu and F. Wilczek, "Interior Gap Superfluidity," Phys. Rev. Lett. **90,** 047002 (2003).

[14] S.-T. Wu and S. Yip, "Superfluidity in the interior-gap states," Phys. Rev. A **67,** 053603 (2003).

[15] J. Carlson and S. Reddy, "Asymmetric Two-Component Fermion Systems in Strong Coupling," Phys. Rev. Lett. **95,** 060401 (2005).

[16] T.-L. Dao, M. Ferrero, A. Georges, M. Capone, and O. Parcollet, "Polarized Superfluidity in the Attractive Hubbard Model with Population Imbalance," Phys. Rev. Lett. **101,** 236405 (2008).

[17] Y.-i. Shin, C. H. Schunck, A. Schirotzek, and W. Ketterle, "Phase diagram of a two-component Fermi gas with resonant interactions," Nature **451,** 689–693 (2008).

[18] P. Fulde and R. A. Ferrell, "Superconductivity in a Strong Spin-Exchange Field," Phys. Rev. **135,** A550–A563 (1964).

[19] A. I. Larkin and Y. N. Ovchinnikov, "Inhomogeneous state of superconductivity," Zh. Eksp. Teor. Fiz. **47,** 1136–1146 (1964), [Sov. Phys. JETP 20, 762 (1965)].

[20] M. Alford, J. A. Bowers, and K. Rajagopal, "Crystalline color superconductivity," Phys. Rev. D **63,** 074016 (2001).

[21] D. F. Agterberg, M. Sigrist, and H. Tsunetsugu, "Order Parameter and Vortices in the Superconducting Q Phase of $CeCoIn_5$," Phys. Rev. Lett. **102,** 207004 (2009).

[22] Y.-a. Liao, A. S. C. Rittner, T. Paprotta, W. Li, G. B. Partridge, R. G. Hulet, S. K. Baur, and E. J. Mueller, "Spin-imbalance in a one-dimensional Fermi gas," Nature **467,** 567–569 (2010).

[23] L. Radzihovsky, "Fluctuations and phase transitions in Larkin-Ovchinnikov liquid-crystal states of a population-imbalanced resonant Fermi gas," Phys. Rev. A **84,** 023611 (2011).

[24] J. Kajala, F. Massel, and P. Törmä, "Expansion dynamics of the Fulde-Ferrell-Larkin-Ovchinnikov state," Phys. Rev. A **84,** 041601 (2011).

[25] Z. Cai, Y. Wang, and C. Wu, "Stable Fulde-Ferrell-Larkin-Ovchinnikov pairing states in two-dimensional and three-dimensional optical lattices," Phys. Rev. A **83,** 063621 (2011).

[26] A. Bulgac, M. M. Forbes, and A. Schwenk, "Induced P-Wave Superfluidity in Asymmetric Fermi Gases," Phys. Rev. Lett. **97,** 020402 (2006).

[27] W. Kohn and L. J. Sham, "Self-Consistent Equations Including Exchange and Correlation Effects," Phys. Rev. **140,** A1133–A1138 (1965).

[28] K. Machida and H. Nakanishi, "Superconductivity under a ferromagnetic molecular field," Phys. Rev. B **30,** 122–133 (1984).

[29] A. Buzdin and S. Polonskii, "Nonuniform state in quasi-1D superconductors," Sov. Phys. JETP **66,** 422 (1987).

[30] K. Yang, "Inhomogeneous superconducting state in quasi-one-dimensional systems," Phys. Rev. B **63,** 140511 (2001).

[31] E. Zhao and W. V. Liu, "Theory of quasi-one-dimensional imbalanced Fermi gases," Phys. Rev. A **78,** 063605 (2008).

[32] G. Orso, "Attractive Fermi Gases with Unequal Spin Populations in Highly Elongated Traps," Phys. Rev. Lett. **98,** 070402 (2007).

[33] H. Hu, X.-J. Liu, and P. D. Drummond, "Phase Diagram of a Strongly Interacting Polarized Fermi Gas in One Dimension," Phys. Rev. Lett. **98,** 070403 (2007).

[34] P. Kakashvili and C. J. Bolech, "Paired states in spin-imbalanced atomic Fermi gases in one dimension," Phys. Rev. A **79,** 041603 (2009).

[35] G. G. Batrouni, M. H. Huntley, V. G. Rousseau, and R. T. Scalettar, "Exact Numerical Study of Pair Formation with Imbalanced Fermion Populations," Phys. Rev. Lett. **100,** 116405 (2008).

[36] M. Casula, D. M. Ceperley, and E. J. Mueller, "Quantum Monte Carlo study of one-dimensional trapped fermions with attractive contact interactions," Phys. Rev. A **78,** 033607 (2008).

[37] T. Roscilde, M. RodrÃŋguez, K. Eckert, O. Romero-Isart, M. Lewenstein, E. Polzik, and A. Sanpera, "Quantum polarization spectroscopy of correlations in attractive fermionic gases," New Journal of Physics **11,** 055041 (2009).

[38] A. E. Feiguin and F. Heidrich-Meisner, "Pairing states of a polarized Fermi gas trapped in a one-dimensional optical lattice," Phys. Rev. B **76,** 220508 (2007).

[39] M. Tezuka and M. Ueda, "Density-Matrix Renormalization Group Study of Trapped Imbalanced Fermi Condensates," Phys. Rev. Lett. **100,** 110403 (2008).

[40] M. Machida, S. Yamada, M. Okumura, Y. Ohashi, and H. Matsumoto, "Correlation effects on atom-density profiles of one- and two-dimensional polarized atomic Fermi gases loaded on an optical lattice," Phys. Rev. A **77,** 053614 (2008).

[41] M. Rizzi, M. Polini, M. A. Cazalilla, M. R. Bakhtiari, M. P. Tosi, and R. Fazio, "Fulde-Ferrell-Larkin-Ovchinnikov pairing in one-dimensional optical lattices," Phys. Rev. B **77,** 245105 (2008).

[42] A. Lüscher, R. M. Noack, and A. M. Läuchli, "Fulde-Ferrell-Larkin-Ovchinnikov state in the one-dimensional attractive Hubbard model and its fingerprint in spatial noise correlations," Phys. Rev. A **78,** 013637 (2008).

[43] F. Heidrich-Meisner, G. Orso, and A. E. Feiguin, "Phase separation of trapped spin-imbalanced Fermi gases in one-dimensional optical lattices," Phys. Rev. A **81,** 053602 (2010).

[44] M. Tezuka and M. Ueda, "Ground states and dynamics of population-imbalanced Fermi condensates in one dimension," New Journal of Physics **12,** 055029 (2010).

[45] G. Xianlong and R. Asgari, "Spin-density-functional theory for imbalanced interacting Fermi gases in highly elongated harmonic traps," Phys. Rev. A **77,** 033604 (2008).

[46] E. A. Cornell and C. E. Wieman, "Nobel Lecture: Bose-Einstein condensation in a dilute gas, the first 70 years and some recent experiments," Rev. Mod. Phys. **74,** 875–893 (2002).

[47] W. Ketterle, "Nobel lecture: When atoms behave as waves: Bose-Einstein condensation and the atom laser," Rev. Mod. Phys. **74,** 1131–1151 (2002).

[48] B. DeMarco and D. S. Jin, "Onset of Fermi Degeneracy in a Trapped Atomic Gas," Science **285,** 1703–1706 (1999).

[49] S. Jochim, M. Bartenstein, A. Altmeyer, G. Hendl, S. Riedl, C. Chin, J. Hecker Denschlag, and R. Grimm, "Bose-Einstein Condensation of Molecules," Science **302,** 2101–2103 (2003).

[50] M. Greiner, C. A. Regal, and D. S. Jin, "Emergence of a molecular Bose–Einstein condensate from a Fermi gas," Nature **426,** 537–540 (2003).

[51] M. W. Zwierlein, C. A. Stan, C. H. Schunck, S. M. F. Raupach, S. Gupta, Z. Hadzibabic, and W. Ketterle, "Observation of Bose-Einstein Condensation of Molecules," Phys. Rev. Lett. **91,** 250401 (2003).

[52] M. W. Zwierlein, A. Schirotzek, C. H. Schunck, and W. Ketterle, "Fermionic Superfluidity with Imbalanced Spin Populations," Science **311,** 492–496 (2006).

[53] G. B. Partridge, W. Li, R. I. Kamar, Y.-a. Liao, and R. G. Hulet, "Pairing and Phase Separation in a Polarized Fermi Gas," Science **311,** 503–505 (2006).

[54] A. Bianchi, R. Movshovich, C. Capan, P. G. Pagliuso, and J. L. Sarrao, "Possible Fulde-Ferrell-Larkin-Ovchinnikov Superconducting State in $CeCoIn_5$," Phys. Rev. Lett. **91,** 187004 (2003).

[55] H. Radovan, N. Fortune, T. Murphy, S. Hannahs, E. Palm, S. Tozer, and D. Hall, "Magnetic enhancement of superconductivity from electron spin domains," Nature **425,** 51–55 (2003).

[56] R. Casalbuoni and G. Nardulli, "Inhomogeneous superconductivity in condensed matter and QCD," Rev. Mod. Phys. **76,** 263–320 (2004).

[57] H. Shimahara, "Fulde-Ferrell state in quasi-two-dimensional superconductors," Phys. Rev. B **50,** 12760–12765 (1994).

[58] H. Shimahara, "Fulde-Ferrell-Larkin-Ovchinnikov State in a Quasi-Two-Dimensional Organic Superconductor," Journal of the Physical Society of Japan **66,** 541–544 (1997).

[59] H. Burkhardt and D. Rainer, "Fulde-Ferrell-Larkin-Ovchinnikov state in layered superconductors," Annalen der Physik **506,** 181–194 (1994).

[60] J. Singleton, J. A. Symington, M.-S. Nam, A. Ardavan, M. Kurmoo, and P. Day, "Observation of the Fulde-Ferrell-Larkin-Ovchinnikov state in the quasi-two-dimensional organic superconductor $\kappa-(\text{BEDT-TTF})_2\text{Cu}(\text{NCS})_2$ (BEDT-TTF=bis(ethylene-dithio)tetrathiafulvalene)," Journal of Physics: Condensed Matter **12,** L641 (2000).

[61] M. A. Tanatar, T. Ishiguro, H. Tanaka, and H. Kobayashi, "Magnetic field-temperature phase diagram of the quasi-two-dimensional organic superconductor $\lambda-(\text{BETS})_2\text{GaCl}_4$ studied via thermal conductivity," Phys. Rev. B **66,** 134503 (2002).

[62] S. Uji *et al.*, "Vortex Dynamics and the Fulde-Ferrell-Larkin-Ovchinnikov State in a Magnetic-Field-Induced Organic Superconductor," Phys. Rev. Lett. **97,** 157001 (2006).

[63] L. Balicas, J. S. Brooks, K. Storr, S. Uji, M. Tokumoto, H. Tanaka, H. Kobayashi, A. Kobayashi, V. Barzykin, and L. P. Gor'kov, "Superconductivity in an Organic Insulator at Very High Magnetic Fields," Phys. Rev. Lett. **87,** 067002 (2001).

[64] M. Houzet, A. Buzdin, L. Bulaevskii, and M. Maley, "New Superconducting Phases in Field-Induced Organic Superconductor $\lambda - (\mathrm{BETS})_2\mathrm{FeCl}_4$," Phys. Rev. Lett. **88,** 227001 (2002).

[65] R. Lortz, Y. Wang, A. Demuer, P. H. M. Böttger, B. Bergk, G. Zwicknagl, Y. Nakazawa, and J. Wosnitza, "Calorimetric Evidence for a Fulde-Ferrell-Larkin-Ovchinnikov Superconducting State in the Layered Organic Superconductor $\kappa - (\mathrm{BEDT\text{-}TTF})_2\mathrm{Cu}(\mathrm{NCS})_2$," Phys. Rev. Lett. **99,** 187002 (2007).

[66] H. Bethe, "Zur Theorie der Metalle," Zeitschrift für Physik **71,** 205–226 (1931).

[67] S. A. Hartnoll, "Lectures on holographic methods for condensed matter physics," Class. Quant. Grav. **26,** 224002 (2009).

[68] S. Sachdev, "What Can Gauge-Gravity Duality Teach Us About Condensed Matter Physics?," Annual Review of Condensed Matter Physics **3,** 9–33 (2012).

[69] A. Green, "An introduction to gauge-gravity duality and its application in condensed matter," Contemporary Physics **54,** 33–48 (2013).

[70] J. McGreevy, "Holographic duality with a view toward many-body physics," Adv.High Energy Phys. **2010,** 723105 (2010).

[71] S. A. Hartnoll, C. P. Herzog, and G. T. Horowitz, "Building a Holographic Superconductor," Phys. Rev. Lett. **101,** 031601 (2008).

[72] S. A. Hartnoll, C. P. Herzog, and G. T. Horowitz, "Holographic Superconductors," JHEP **0812,** 015 (2008).

[73] J. Erdmenger, V. Grass, P. Kerner, and T. H. Ngo, "Holographic Superfluidity in Imbalanced Mixtures," JHEP **1108,** 037 (2011).

[74] F. Bigazzi, A. L. Cotrone, D. Musso, N. P. Fokeeva, and D. Seminara, "Unbalanced Holographic Superconductors and Spintronics," JHEP **1202,** 078 (2012).

[75] M. M. Forbes, E. Gubankova, W. V. Liu, and F. Wilczek, "Stability Criteria for Breached-Pair Superfluidity," Phys. Rev. Lett. **94,** 017001 (2005).

[76] K. Machida, T. Mizushima, and M. Ichioka, "Generic Phase Diagram of Fermion Superfluids with Population Imbalance," Phys. Rev. Lett. **97,** 120407 (2006).

[77] H. Hu and X.-J. Liu, "Mean-field phase diagrams of imbalanced Fermi gases near a Feshbach resonance," Phys. Rev. A **73,** 051603 (2006).

[78] S. Pilati and S. Giorgini, "Phase Separation in a Polarized Fermi Gas at Zero Temperature," Phys. Rev. Lett. **100,** 030401 (2008).

[79] M. W. Zwierlein, C. H. Schunck, A. Schirotzek, and W. Ketterle, "Direct observation of the superfluid phase transition in ultracold Fermi gases," nature **442,** 54–58 (2006).

[80] Y. Shin, M. W. Zwierlein, C. H. Schunck, A. Schirotzek, and W. Ketterle, "Observation of Phase Separation in a Strongly Interacting Imbalanced Fermi Gas," Phys. Rev. Lett. **97,** 030401 (2006).

[81] C. H. Schunck, Y. Shin, A. Schirotzek, M. W. Zwierlein, and W. Ketterle, "Pairing Without Superfluidity: The Ground State of an Imbalanced Fermi Mixture," Science **316,** 867–870 (2007).

[82] G. B. Partridge, W. Li, Y. A. Liao, R. G. Hulet, M. Haque, and H. T. C. Stoof, "Deformation of a Trapped Fermi Gas with Unequal Spin Populations," Phys. Rev. Lett. **97,** 190407 (2006).

[83] K. Maki and T. Tsuneto, "Pauli Paramagnetism and Superconducting State," Progress of Theoretical Physics **31,** 945–956 (1964).

[84] M. M. Parish, F. Marchetti, A. Lamacraft, and B. Simons, "Finite-temperature phase diagram of a polarized Fermi condensate," Nature Physics **3,** 124–128 (2007).

[85] E. I. Blount and C. M. Varma, "Electromagnetic Effects near the Superconductor-to-Ferromagnet Transition," Phys. Rev. Lett. **42,** 1079–1082 (1979).

[86] D. E. Sheehy, "Polarized superfluids near their tricritical point," Phys. Rev. A **79,** 033606 (2009).

[87] D. Agterberg and K. Yang, "The effect of impurities on Fulde-Ferrell-Larkin-Ovchinnikov superconductors," Journal of Physics: Condensed Matter **13,** 9259 (2001).

[88] A. Buzdin and H. Kachkachi, "Generalized Ginzburg-Landau theory for nonuniform FFLO superconductors," Physics Letters A **225,** 341 – 348 (1997).

[89] R. Combescot and C. Mora, "Transition to Fulde-Ferrel-Larkin-Ovchinnikov phases near the tricritical point: an analytical study," The European Physical Journal B - Condensed Matter and Complex Systems **28,** 397–406 (2002).

[90] B.-L. Young, R. R. Urbano, N. J. Curro, J. D. Thompson, J. L. Sarrao, A. B. Vorontsov, and M. J. Graf, "Microscopic Evidence for Field-Induced Magnetism in $CeCoIn_5$," Phys. Rev. Lett. **98,** 036402 (2007).

[91] M. Kenzelmann *et al.*, "Coupled Superconducting and Magnetic Order in CeCoIn5," Science **321,** 1652–1654 (2008).

[92] G. Koutroulakis, M. D. Stewart, V. F. Mitrović, M. Horvatić, C. Berthier, G. Lapertot, and J. Flouquet, "Field Evolution of Coexisting Superconducting and Magnetic Orders in $CeCoIn_5$," Phys. Rev. Lett. **104,** 087001 (2010).

[93] K. Kumagai, H. Shishido, T. Shibauchi, and Y. Matsuda, "Evolution of Paramagnetic Quasiparticle Excitations Emerged in the High-Field Superconducting Phase of $CeCoIn_5$," Phys. Rev. Lett. **106,** 137004 (2011).

[94] B. Bergk, A. Demuer, I. Sheikin, Y. Wang, J. Wosnitza, Y. Nakazawa, and R. Lortz, "Magnetic torque evidence for the Fulde-Ferrell-Larkin-Ovchinnikov state in the layered organic superconductor $\kappa-(\text{BEDT-TTF})_2\text{Cu(NCS)}_2$," Phys. Rev. B **83,** 064506 (2011).

[95] J. A. Wright, E. Green, P. Kuhns, A. Reyes, J. Brooks, J. Schlueter, R. Kato, H. Yamamoto, M. Kobayashi, and S. E. Brown, "Zeeman-Driven Phase Transition within the Superconducting State of $\kappa-(\text{BEDT-TTF})_2\text{Cu(NCS)}_2$," Phys. Rev. Lett. **107,** 087002 (2011).

[96] R. Beyer, B. Bergk, S. Yasin, J. A. Schlueter, and J. Wosnitza, "Angle-Dependent Evolution of the Fulde-Ferrell-Larkin-Ovchinnikov State in an Organic Superconductor," Phys. Rev. Lett. **109,** 027003 (2012).

[97] M. D. Croitoru and A. I. Buzdin, "Resonance in-plane magnetic field effect as a means to reveal the Fulde-Ferrell-Larkin-Ovchinnikov state in layered superconductors," Phys. Rev. B **86,** 064507 (2012).

[98] M. D. Croitoru, M. Houzet, and A. I. Buzdin, "In-Plane Magnetic Field Anisotropy of the Fulde-Ferrell-Larkin-Ovchinnikov State in Layered Superconductors," Phys. Rev. Lett. **108,** 207005 (2012).

[99] A. Aharony, E. Domany, and R. M. Hornreich, "Renormalization-group analysis of Lifshitz tricritical behavior," Phys. Rev. B **36,** 2006–2014 (1987).

[100] A. A. Abrikosov, L. P. Gor'kov, and I. E. Dzyaloshinski, *Methods of Quantum Field Theory in Statistical Physics*, revised ed. (Dover Publications, 1975).

[101] F. Konschelle, J. Cayssol, and A. I. Buzdin, "Anomalous fluctuation regimes at FFLO transition," Europhysics Letters **79,** 67001 (2007).

[102] I. Sodemann, D. A. Pesin, and A. H. MacDonald, "Density, spin, and pairing instabilities in polarized ultracold Fermi gases," Phys. Rev. A **85,** 033628 (2012).

[103] A. Bray, "Theory of phase-ordering kinetics," Advances in Physics **43,** 357–459 (1994).

[104] A. Basu and J. K. Bhattacharjee, "Scaling in a temperature quench in systems with a Lifshitz point: nonconserved and conserved order parameters," Journal of Physics A: Mathematical and General **37,** 1111 (2004).

[105] J. D. Bekenstein, "Black holes and entropy," Phys. Rev. D **7,** 2333–2346 (1973).

[106] S. Hawking, "Particle Creation by Black Holes," Commun. Math. Phys. **43,** 199–220 (1975).

[107] G. 't Hooft, "Dimensional reduction in quantum gravity," arXiv gr-qc/9310026 (1993).

[108] L. Susskind, "The World as a hologram," J. Math. Phys. **36,** 6377–6396 (1995).

[109] W. Fischler and L. Susskind, "Holography and cosmology," arXiv hep-th/9806039 (1998).

[110] D. Bigatti and L. Susskind, "TASI lectures on the holographic principle," arXiv hep-th/0002044 pp. 883–933 (1999).

[111] J. M. Maldacena, "The Large N limit of superconformal field theories and supergravity," Adv. Theor. Math. Phys. **2,** 231–252 (1998).

[112] G. 't Hooft, "A Planar Diagram Theory for Strong Interactions," Nucl. Phys. B **72,** 461 (1974).

[113] E. Witten, "Anti-de Sitter space and holography," Adv. Theor. Math. Phys. **2,** 253–291 (1998).

[114] O. Aharony, S. S. Gubser, J. M. Maldacena, H. Ooguri, and Y. Oz, "Large N field theories, string theory and gravity," Phys. Rept. **323,** 183–386 (2000).

[115] E. D'Hoker and D. Z. Freedman, "Supersymmetric gauge theories and the AdS / CFT correspondence," arXiv hep-th/0201253 pp. 3–158 (2002).

[116] J. Erdmenger, N. Evans, I. Kirsch, and E. Threlfall, "Mesons in Gauge/Gravity Duals - A Review," Eur. Phys. J. A **35,** 81–133 (2008).

[117] S. Ryu and T. Takayanagi, "Holographic derivation of entanglement entropy from AdS/CFT," Phys. Rev. Lett. **96,** 181602 (2006).

[118] S. Ryu and T. Takayanagi, "Aspects of Holographic Entanglement Entropy," JHEP **0608,** 045 (2006).

[119] D. V. Fursaev, "Proof of the holographic formula for entanglement entropy," JHEP **0609,** 018 (2006).

[120] M. Headrick, "Entanglement Renyi entropies in holographic theories," Phys. Rev. D **82,** 126010 (2010).

[121] H. Casini and M. Huerta, "Positivity, entanglement entropy, and minimal surfaces," JHEP **1211,** 087 (2012).

[122] T. Nishioka, S. Ryu, and T. Takayanagi, "Holographic Entanglement Entropy: An Overview," J. Phys. A **42,** 504008 (2009).

[123] T. Takayanagi, "Entanglement Entropy from a Holographic Viewpoint," Class. Quant. Grav. **29,** 153001 (2012).

[124] T. Albash and C. V. Johnson, "Holographic Studies of Entanglement Entropy in Superconductors," JHEP **1205,** 079 (2012).

[125] T. Albash and C. V. Johnson, "Evolution of Holographic Entanglement Entropy after Thermal and Electromagnetic Quenches," New J. Phys. **13,** 045017 (2011).

[126] R.-G. Cai, S. He, L. Li, and Y.-L. Zhang, "Holographic Entanglement Entropy on P-wave Superconductor Phase Transition," JHEP **1207,** 027 (2012).

[127] R.-G. Cai, L. Li, L.-F. Li, and R.-K. Su, "Entanglement Entropy in Holographic P-Wave Superconductor/Insulator Model," JHEP **1306,** 063 (2013).

[128] N. P. Fokeeva, Master's thesis, Universitá degli studi di Firenze, Florence, Italy, 2011.

[129] J. Alsup, E. Papantonopoulos, and G. Siopsis, "A Novel Mechanism to Generate FFLO States in Holographic Superconductors," Phys. Lett. B **720,** 379–384 (2013).

[130] J. Alsup, E. Papantonopoulos, and G. Siopsis, "FFLO States in Holographic Superconductors," arXiv 1208.4582 (2012).

[131] J. Alsup, E. Papantonopoulos, G. Siopsis, and K. Yeter, "Spontaneously Generated Inhomogeneous Phases via Holography," arXiv 1305.2507 (2013).

[132] T. Hertog, "Towards a Novel no-hair Theorem for Black Holes," Phys. Rev. D **74,** 084008 (2006).

[133] S. S. Gubser, "Breaking an Abelian gauge symmetry near a black hole horizon," Phys. Rev. D **78,** 065034 (2008).

[134] R. Banerjee, S. K. Modak, and D. Roychowdhury, "A unified picture of phase transition: from liquid-vapour systems to AdS black holes," JHEP **1210,** 125 (2012).